The University of Chicago

SOME ASPECTS OF B-TYPE SPECTRA

A DISSERTATION SUBMITTED TO THE FACULTY
OF THE DIVISION OF THE PHYSICAL SCIENCES
IN CANDIDACY FOR THE DEGREE OF DOCTOR
OF PHILOSOPHY

DEPARTMENT OF ASTRONOMY AND ASTROPHYSICS
1948

By
ANNE B. UNDERHILL

Reprinted from
The Astrophysical Journal
Vol. 107, No. 2, March, 1948; Vol. 107, No. 3, May, 1948

The University of Chicago

SOME ASPECTS OF B-TYPE SPECTRA

A DISSERTATION SUBMITTED TO THE FACULTY
OF THE DIVISION OF THE PHYSICAL SCIENCES
IN CANDIDACY FOR THE DEGREE OF DOCTOR
OF PHILOSOPHY

DEPARTMENT OF ASTRONOMY AND ASTROPHYSICS
1948

By
ANNE B. UNDERHILL

Reprinted from
The Astrophysical Journal
Vol. 107, No. 2, March, 1948; Vol. 107, No. 3, May, 1948

2778/49

SOME ASPECTS OF B-TYPE SPECTRA

INTRODUCTION

The study of stellar atmospheres can be attacked from two viewpoints: the observational and the theoretical. The observational approach is to obtain quantitative answers to the three questions: what atoms or ions are represented in the stellar spectrum, what are the relative strengths of the lines, and what are the shapes of the lines? The theoretical approach is to make some definite hypotheses about the physical and chemical structure of a stellar atmosphere and then to predict the stellar spectrum from the physical theory of atoms, and from the theory of the transfer of radiation in a stellar atmosphere. We say that the model atmosphere which reconciles predictions and observations in detail represents the physical and chemical structure of the stellar atmosphere.

Such a study has been undertaken for B-type stars, and the procedures and results are given in three papers: "The Spectrum of γ Pegasi," "The Intensities and Profiles of Lines in Some B-Type Stars," and "The Schuster-Problem for an Extended Atmosphere."

The first paper represents an attempt at the measurement and identification of all the lines present in a B2.5 main-sequence star; it is therefore an answer to the first quantitative question.

The second paper provides quantitative answers to the second and third questions for some of the strongest lines in B-type spectra. Observation and theory are compared, and two model atmospheres are calculated.

The third paper is entirely theoretical. The present theory of stellar atmospheres postulates atmospheres stratified in plane-parallel layers and, although it is likely that this approximation is adequate for the discussion of the atmospheres of main-sequence stars, it may not be sufficient for the discussion of the atmospheres of supergiant stars. A simple problem of line formation in a spherically symmetric atmosphere is investigated and some conclusions regarding the effect of extent of atmosphere on the predicted line profile and equivalent width are given.

THE SPECTRUM OF γ PEGASI*

ANNE B. UNDERHILL†
Yerkes and McDonald Observatories
Received November 19, 1947

ABSTRACT

Two coudé plates of γ Pegasi have been measured for wave length, and some new lines were found. About 70 per cent of the 877 lines measured between λ 3965 and λ 4921 have been identified. The results show generally that the spectrum of any element of reasonably high abundance on the earth may be found if its excitation potential is around 20–25 volts. Potassium has not been found, in spite of the fact that it is abundant on the earth, and the lines of the *K* II spectrum have very favorable wave length and excitation potential for appearance in γ Pegasi.

Small displacements, such as are qualitatively expected on the basis of Stark effect, are found for the *He* I lines. A quantitative comparison is made between theory and observation, and it is shown that the observed displacements of the diffuse-series lines are more nearly in agreement with those calculated by M. K. Krogdahl on the basis of collisional broadening than with those given by the theory of Stark effect from constant fields.

Some forbidden *He* I lines of the $2^1P - m^1P$ series are tentatively identified, and a possible explanation of a small luminosity effect at λ 4026 between dwarf and intermediate B-type stars is proffered.

I. THE MEASUREMENT AND IDENTIFICATION OF LINES IN γ PEGASI

The star γ Pegasi—$\alpha(1900) = 0^h08^m$; $\delta(1900) = +14°38'$; mag. 2.9—is classified on the system of the Yerkes spectral atlas[1] as B2.5 IV. The lines are very sharp and of excellent quality for measurement. Four plates of γ Pegasi taken by W. A. Hiltner with the coudé spectrograph of the McDonald Observatory in November and December, 1943, were very kindly offered for study. Three of the spectra run from about λ 3965 to λ 4713, and one goes from λ 4068 to λ 4935. The dispersion is 1.82 A/mm at $H\epsilon$, 2.29 at $H\delta$, 3.26 at $H\gamma$, and 5.82 at $H\beta$. The plates are of exquisite quality, the spectra being wide and in excellent focus and definition throughout their entire length. A visual inspection of the plates revealed so many more faint features than had previously been reported in the spectrum of γ Pegasi that it seemed worth while to measure the two best plates for wave length, attempting to record every feature. The plates were measured in one direction only, two independent series of measures being made and reduced separately. In compiling the final list of lines, the reality of each feature was checked by visual inspection of all the plates on which it should appear.

The settings, before reduction to wave length, were corrected for the radial velocity of the star as determined from the *He* I lines, the *H* lines, and the strong lines of *O*, *N*, and *Si*. Hence, if there are peculiar displacements of the *He* I and *H* lines with respect to the other lines, a systematic error will be introduced in the measured wave lengths. To investigate such peculiar displacements, which might arise from personal bias in bisecting very strong lines (this effect was not minimized by reversing the plate) or from physical causes, the lines were grouped as indicated in Table 1, and the average residual $\lambda_{star} - \lambda_{lab}$ found for each group. It is evident that the *H* and *He* I lines are displaced to the red with respect to the other lines and that a mean correction of +0.016 A is required to reduce the measured wave lengths to zero velocity. Such a correction has been incorporated in the table of wave lengths. The *He* displacements are discussed later; the *H* displacements may be fictitious because of personal bias.

* *Contributions from the McDonald Observatory, University of Texas*, No. 146.

† This work was completed during the author's tenure of a scholarship from the Canadian Federation of University Women.

[1] Morgan, Keenan, and Kellman, *An Atlas of Stellar Spectra* (Chicago: University of Chicago Press, 1943).

The estimated intensities, mean wave lengths, and identifications are given in Table 2. The intensity scale runs from 00 for lines on the verge of visibility to about 10 for strong sharp lines. Occasionally, the remark "diffuse, *n*," is made. In general, the lines are very sharp, diffuseness usually indicating a forbidden line or an unresolved blend. Lines marked as *n* in the laboratory appear to be as sharp as any of the other lines. In particular, the lines of *N* II, specially mentioned by Struve[2] because of their diffuse character in the laboratory, are found to be just as sharp as the other lines. Laboratory intensities are given in parentheses after the laboratory wave lengths.

Table 2 has been compared to the list of lines given by Kühlborn[3] in five wave-length regions: λλ 4050–4090, λλ 4267–4307, λλ 4395–4431, λλ 4612–4664, λλ 4792–4902. The average $\lambda_{star}-\lambda_{lab}$ for these regions in Table 2 is ± 0.058 A; in Kühlborn's table it is ± 0.080 A. Owing partly to the improved and increased spectroscopic knowledge now available, about 70 per cent of the lines in Table 2 have been identified, whereas Kühlborn identifies only about 50 per cent. In the region $4200 < \lambda < 4700$ the number of lines measured by both of us is about the same, the chief advantage of Table 2 being the greater number of identifications, mostly *Fe* III, that are made. For the region $\lambda < 4100$, Table 2 is notable for the very small number of unidentified lines remaining. In this

TABLE 1

AVERAGE RESIDUALS

Group	$\lambda_{star}-\lambda_{lab}$
1. All lines used for radial velocity	+0.003A
2. All *H* lines	+ .000
3. All *He* lines of intensity > 2	+ .040
4. All other lines of intensity > 2	− .016
5. All lines of intensity 1–2	− .017
6. All lines of intensity 0	− .022
7. All lines of intensity 00	− .015
8. All radial-velocity lines except *He* and *H*	−0.015

region Kühlborn lists twice as many lines as are given in Table 2 but makes only the same identification as in Table 2; thus half his lines are unidentified. In this region he has a density of lines which is three times what he finds (and approximately what I find) for $\lambda > 4100$. It would seem probable that some of Kühlborn's lines in the region $\lambda < 4100$ are spurious. For the region $\lambda > 4700$ Kühlborn's list of lines is very meager, the comparison having been made chiefly against lines that he measures in other B-type stars. The percentage of unidentified lines in Table 2 for this region is a little larger than it is for the rest of the table, being 39.6 per cent. The wave lengths are from the measurement of a Mount Wilson coudé plate of this region (dispersion 2.83 A/mm) taken by H. W. Babcock and from one McDonald coudé plate.

Figures 1 and 2 show the spectrum of γ Pegasi. Comparison with other published spectra of B-type stars[4] shows the superiority of the present material for studying faint features and for general definition and resolution.

All coincidences within ± 0.08 A ($\lambda < 4700$ A) and ± 0.15 A ($\lambda > 4700$ A) with lines in the finding list[5] were tabulated for elements of the expected level of ionization and excitation. The mean level of ionization and excitation in γ Pegasi lies near 21 volts,[2,3,4] and it is found that, if the ionization potential of an atom and the excitation potential of the lower levels of the lines in the next spectrum lie between 15 and about 25 volts,

[2] *Ap. J.*, **74**, 225, 1931.

[3] *Veröff. U.-Sternw. Berlin-Babelsberg*, Vol. **12**, No. 1, 1938.

[4] E.g., *Ap. J.*, **74**, 225, 1931; also R. K. Marshall, *Pub. Michigan Obs.*, **5**, 137, 1934.

[5] C. Moore, *Contr. Princeton U. Obs.*, No. 20, Parts I and II, 1945.

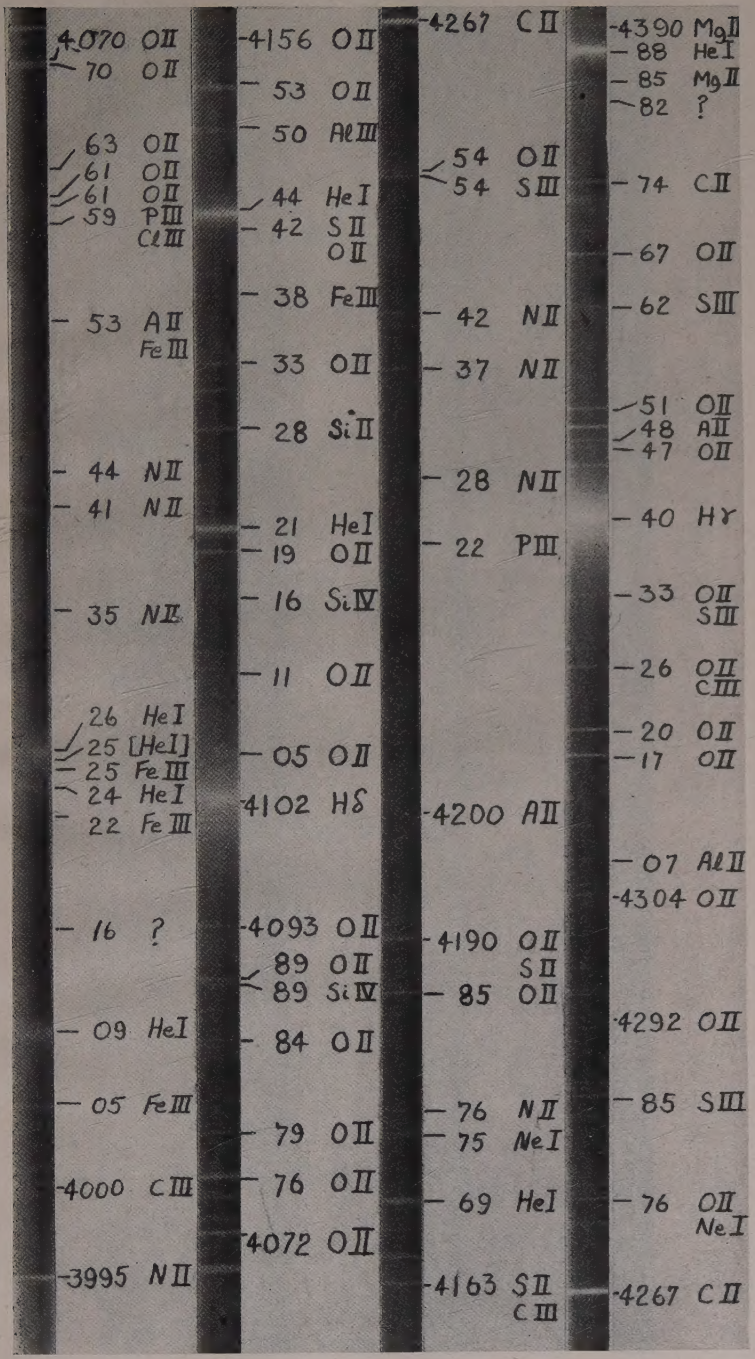

FIG. 1.—The spectrum of γ Pegasi

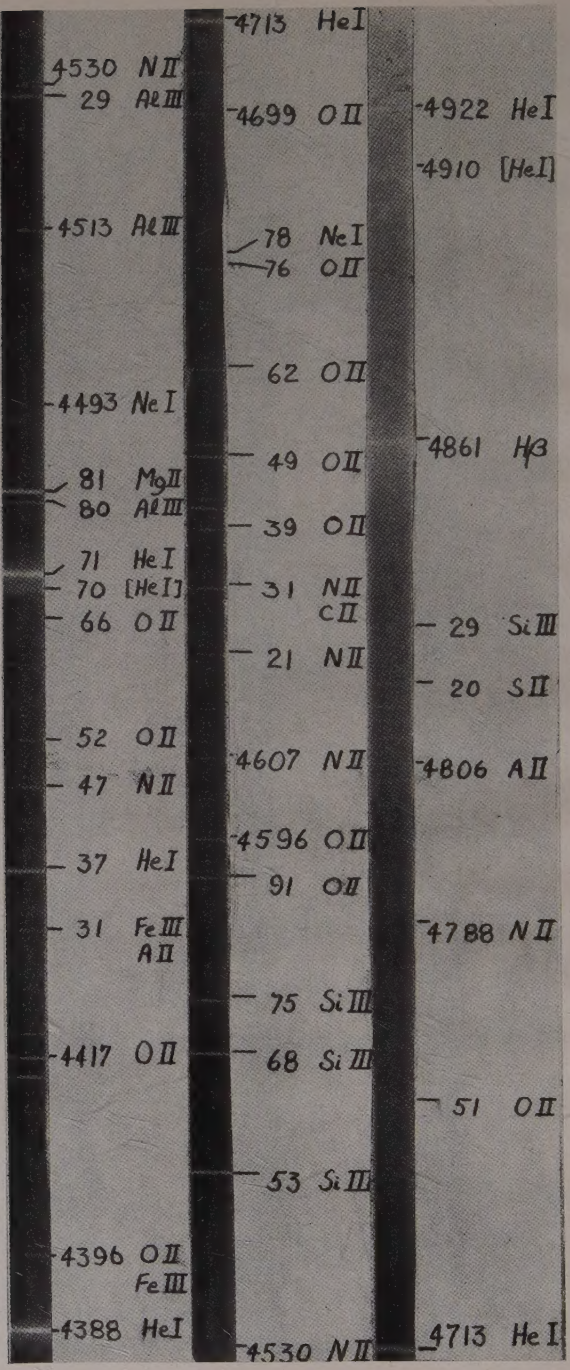

FIG. 2.—The spectrum of γ Pegasi

TABLE 2.

LINES IN γ PEGASI

λ	Int.	Identification	λ	Int.	Identification	λ	Int.	Identification
3964.68	10	He I .73(4)	4032.71	0	S II .81(7)	4087.72	00	FeIII .76(tr)
67.68	0	O II .44(1)	33.15	0	O II .18(0d)			NaII .60(0)
68.42	5	CaII .47(350)	33.74	00	P II .68(2)	88.31	00	FeIII .55(2)
70.15	100	H .07(Hε)			A II .83(6)			.16(tr)
72.42	0	C II .44(0)	35.04	1	N II .09(4n)	88.87	1	SiIV .86(10)
73.25	1	O II .26(10)			O II .09(0d)	89.34	2	O II .30(4n)
73.86	00	C II .84(1d)	35.37	0	A II .47(6)	92.96	2	O II .94(5)
74.26	00	A II .48(5)	39.05	0	FeII .12(3)	93.50	00	FeIII .36(2)
74.64	00	A II .76(6)	41.40	2	N II .32(5n)	94.22	0	O II .18(0)
75.17	0	FeIII .13(4)			O II .31(0d)	94.80	00	....
75.76	00	....	41.92	0	....	95.17	0	S III .17(-)
77.25	00	C II .30(0)	42.90	0	A II .91(8)	95.71	0	O II .63(0n)
78.21	00	P III .28(8)	43.52	2	N II .54(3n)	96.17	00	O II .18(0d)
79.24	0	A II .36(7)	43.98	00	FeIII .05(4)	96.61	0	FeIII .76(3)
80.34	0	C II .35(3)	44.79	1	N II .75(1)			O II .54(3)
81.60	00	....			FeIII .79(1)	97.30	00	O II .26(4n,
82.18	00	....			O II .96(0d)			4n)
82.68	2	O II .72(5)	45.97	0	O II .15(00d)	98.37	00	O II .27(0n)
83.72	1	S III .77(3)	47.37	0	A II .51(3)	4099.61	00	FeIII .56(tr)
84.04	00	?Ne I .06(0.5)	48.06	0	O II .22(1n)			?A II .47(3)
85.99	0	FeIII .00(3)	48.91	0	FeII .88(3)	4100.59	00	FeIII .52(3)
		S III .97(2)	51.09	0	FeIII .08(2)	01.73	100	H .74(Hδ)
87.14	0	....	52.18	0	ClII .22(12)	03.64	00	F II .53(15)
90.87	0	S II .94(3)	53.06	1	A II .94(5)			.72(7)
		FeIII .81(tr)			FeIII .28(5)			.87(7)
91.58	0	ClIII .50(7)	53.94	0	O II .10(0d)	04.09	00	A II .91(10,
93.33	00	FeIII .30(4)	55.20	0	....			10)
		S II .53(4)	56.13	00	C III .06(5)	04.39	00	ClIII .23(5)
94.98	9	N II .00(10)	56.86	0	N II .00(1)	04.89	0	O II .74(5)
		A II .81(5,5)			AlII .8 (0.5)			.00(7)
95.87	00	AlII .86(5)	58.60	0	S II .7 (00)	06.23	00	O II .03(0)
		FeIII .81(1)	59.28	1	P III .27(6)	07.50	0	FeIII .65(3)
96.18	00	AlII .16(4)			ClIII .07(6)	07.97	00	FeIII .12(2)
96.67	0	FeIII .65(tr)	60.58	1	O II .58(3n)	08.44	00	....
97.29	0	P III .17(5)	61.02	1	O II .98(2n)	08.76	00	O II .75(0n)
97.90	0	S III .97(-)	61.72	00	FeII .70(2)	09.59	00	MgII .54(3)
		SiII .00(-)	62.87	1	O II .90(1n)	10.00	00	N II .00(0n)
98.82	0	S II .79(3)	63.91	00	Ne I .04(4)			FeIII .95(5)
3999.90	0	FeIII .83(4)	64.39	00	FeIII .34(1)	10.82	1	O II .80(3)
		C III .92(-)			S III .45(-)	11.46	0	S III .56(-)
4000.60	00	....	65.05	00	A II .14(3)	12.05	1	O II .03(4)
01.21	00	....	66.19	0	FeIII .11(4)			Ne I .10(2)
03.35	0	FeIII .41(4)	68.92	00	C III .97(9)	12.62	0	Ne I .69(2.5)
05.00	2	FeIII .04(-)			Ne I .84(3)	13.29	00	FeIII .45(7)
05.89	0	AlII .7 (0)	69.56	3	O II .64(4)			.23(7)
		FeIII .64(-)	69.89	3	O II .90(6)	13.89	0	O II .82(1)
07.27	0n	[He I] .81(-)	70.29	00	C III .30(10)	14.46	0	A II .52(2)
07.64	0	A II .66(1)	71.20	1	O II .20(0)	15.54	0	....
08.73	0	FeIII .81(5)	72.18	5	O II .16(8)	16.14	1	SiIV .10(8)
09.31	15	He I .27(-)	73.10	0	N II .06(2n)	16.59	00	F II .55(7)
09.96	0	C II .90(2)	74.54	2	C II .53(6)	16.82	0	FeIII .88(3)
11.28	00	A II .23(3)	74.85	2	C II .89(5)	17.45	0	....
13.71	00	?Ne I .75(0)	75.40	0	SiII .45(-)	18.31	0	....
15.80	0	....	75.88	5	O II .87(10)	18.82	0	F II .72(-)
16.43	0	FeIII .47(1)			FeIII .83(3)	19.26	8	O II .22(8)
17.51	0	FeIII .58(3)			C II .00(7)			F II .92(7)
19.96	0	?Ne I .02(0.5)	76.57	00	A II .64(5)	19.86	0	....
21.03	00	C II .13(0)	78.24	00	FeIII .28(1)	20.30	2	O II .28(3)
22.30	1	FeIII .36(4)	78.88	2	O II .86(4)	20.90	15	He I .86(3,1)
24.04	2	He I .99(-)	79.69	00	A II .60(5)			FeIII .97(8)
		O II .04(1n)	80.16	0	Ne I .15(4)	21.52	1	O II .48(4)
24.96	1	FeIII .07(3)			P III .04(7)	22.04	1	FeIII .06(8)
		FeIII .85(2)	81.02	1	?FeIII .19(7)			C III .05(3)
		F II .73(20)			?O III .10(1)	22.76	1	FeIII .98(8)
		F II .01(10)	81.62	0	CaIII .74(5)	23.18	0	Na II .07(3)
25.49	2n	[He I] .40(-)	82.30	1	N II .28(2n)	23.51	00	FeII .50(2)
		.49(-)	82.95	00	N II .85(00)	27.26	00	....
		F II .50(15)	83.90	1	O II .91(2n)	28.06	2	SiII .05(8)
26.24	30	He I .20(5,1)	84.35	00	....			FeIII .06(3)
28.78	0	S II .79(7)	84.63	0	O II .66(1)			Ne I .07(3)
30.03	0	FeIII .04(tr)	85.14	1	O II .12(3)	28.59	00	A II .65(-)
31.35	0	A II .41(2)	87.16	1	O II .6(2n)	29.37	1	O II .34(2)

TABLE 2 -- Continued

λ	Int.	Identification	λ	Int.	Identification	λ	Int.	Identification
4129.92	0	FeIII .95(3)			S II .30(-)	4237.44	00	AlII .57(-)
30.38	00	?Ne I .51(2.5)			Ne I .37(5)	37.93	00	....
30.90	2	Si II .88(10)	4175.12	0	Ne I .22(4.5)	38.60	0	....
		Ne I .05(5)	75.38	0	Ne I .45(3.5)	39.56	00	FeIII .53(1)
31.71	1	A II .73(8)	76.20	2	N II .16(3n)			?O III .5 (00)
32.37	00	ClII .48(200)	76.82	0	FeIII .79(4)	40.00	00	FeIII .06(1)
32.83	2	O II .81(6)	77.33	00	FeIII .19(2)			NeII .95(2)
33.63	0	N II .67(2)	77.77	00	FeIII .63(3)	40.74	0	AlII .75(3)
35.31	00	....	78.35	00	A II .39(5)			FeIII .71(4)
36.97	00	FeIII .95(4)	79.07	00	FeIII .25(5)	41.27	00	....
37.80	1	FeIII .93(10)	79.67	00	N II .67(1n)	41.82	1	N II .79(8n, 8n)
38.27	00	....	80.23	00	....			
39.37	1	FeIII .37(8)	80.75	00	S II .7 (00)	42.50	00	MgII .47(4)
39.99	00	....	84.92	00	....	43.59	00	?B III .60(3d)
40.40	0	FeIII .51(6)	85.48	2	O II .46(8)	44.27	00	?NeII .17(0)
40.95	00	O II .74(0)	85.88	00	S II .95(-)	45.54	00	....
41.46	0	[He I] .34(-)	86.86	0	....	46.08	00	FeIII .18(2)
42.20	0	AlIII .15(2n)	87.93	0	....			F II .16(15n)
		FeIII .16(1)	89.11	0	FeIII .10(7)	46.77	0	FeIII .67(3)
		O II .08(1)	89.77	2	O II .79(10)			P III .68(7)
42.32	1	S II .29(8)			S II .71(6n, 6n)	47.58	00	FeIII .56(2)
		O II .24(0)						C III .56(1)
42.92	0	?[He I] 2P-6G			A II .67(-)	48.15	00	FeIII .11(2)
43.32	0	[He I] .44(-)	91.08	0	FeIII .04(3)	50.78	00	NeII .68(4)
43.86	25	He I .76(2)	91.53	0	?ClII .59(15)	52.42	00	Ne I .42(0.5)
		O II .77(2)	91.81	00	FeIII .96(2)	53.57	2	FeIII .62(4)
		FeIII .87(7)	92.28	00	FeIII .43(2)			S III .59(9)
45.08	1	S II .10(9)	92.57	0	O II .50(2)	54.12	1	FeIII .08(2)
45.91	0	O II .90(0)	93.32	0	....			O II .98(4d)
46.77	0	FeIII .82(4)	94.23	00	FeIII .13(4)	55.02	0	S II .01(0)
		?S II .94(3)	94.92	00	....	55.82	00	....
47.88	00	....	95.99	0	....	57.41	00	S II .42(3)
48.56	00	....	97.18	00	FeIII .29(2)	58.84	00	FeIII .77(2)
49.21	00	....	97.78	00	....	59.68	00	ClII .52(35)
50.07	2n	AlIII .90(10)	98.66	00	....			Ne I .74(0)
		.92(8)	99.44	00	....	60.24	00	....
53.26	3	O II .30(7)	4199.95	0	A II .93(3)	61.47	00	FeIII .46(4)
53.91	00	....	4200.82	00	FeIII .90(1)	62.68	00	....
54.30	00	....	01.89	00	A II .99(5)	63.71	00	FeIII .94(4)
54.92	0	FeIII .98(8)	02.43	00	AlII .4 (2)			.52(4)
55.87	0	FeIII .83(tr)	03.73	00	....	64.53	00	....
56.56	1	O II .54(3)	04.72	00	FeIII .57(4)	65.04	00	....
		C III .50(4)	05.41	00	....	66.58	00	A II .53(10)
57.11	0	....	07.44	00	FeIII .45(2)	67.18	15	C II .02(19)
58.31	00	FeIII .34(3)	08.66	00	FeIII .71(2)			.27(20)
60.42	00	P II .56(3)	10.63	00	....	67.89	0	FeIII .84(2)
62.71	1	S II .70(10, 10)	11.77	00	....			S II .80(5)
		C III .80(5)	12.57	00	SiIV .44(4)	69.11	00	....
63.19	0	....	14.47	00	....	69.70	00	S II .76(3)
64.02	00	....	15.06	00	....			Ne I .72(5)
64.79	1	FeIII .79(20)	15.79	00	?N III .69(3)	71.63	00	....
		Ne I .80(4)	16.41	00	....	73.39	0	FeIII .42(7n)
65.08	0	S II .11(1)	17.30	0	S II .23(3)	74.24	00	O II .13(00)
		S III .96(-)	18.74	00	A II .69(5)	75.53	1	O II .52(4n)
65.60	0	FeIII .53(1)	20.26	00	FeIII .32(5)			Ne I .56(5)
66.18	0	FeIII .09(1)	22.26	1	P III .15(7)	76.00	00	O II .90(0d)
		Ne I .09(3)			FeIII .39(8)	76.74	0	O II .71(1n)
66.86	1	FeIII .86(9)	23.56	00	....	77.44	0	O II .40(1n, 1n)
68.17	0	....	24.00	00	....			
68.42	0	FeIII .41(4)	24.71	00	....	77.98	0	O II .90(1n)
		S II .41(5)	25.43	00	FeIII .39(2)	78.55	0	FeIII .62(1)
69.10	5	He I .97(-)	26.85	00	AlII .83(8)			S II .54(3)
69.76	0	....	27.74	0	N II .75(3n)	79.56	0	FeIII .58(1)
70.32	00	FeIII .34(2)	29.45	00	....	80.66	00	FeIII .74(2)
70.53	00	....	30.97	00	S II .98(4)	81.35	0	O II .40(0n)
71.65	1	N II .61(2n)	31.55	00	FeIII .59(1)	81.98	00	....
72.09	0	FeIII .09(1)			?NeII .60(4)	82.54	00	S II .63(3)
72.53	0	FeIII .58(1)	32.34	00	Ne I .32(0)	83.00	0	A II .90(7)
72.95	0	....	33.72	00	....			O II .96(1n)
73.56	0	N II .51(0n)	34.27	00	FeIII .25(tr)			O II .13(0d)
73.94	0	S II .04(4)	35.56	0	FeIII .54(10)	83.78	0	O II .75(0n)
		Ne I .97(0.5)	36.29	0	....			S III .70(-)
74.27	1	FeIII .27(10)	37.00	2	N II .93(5)	85.00	1	S III .99(5)
					N II .05(4)	85.65	0	O II .70(3n)

TABLE 2 -- Continued

λ	Int.	Identification	λ	Int.	Identification	λ	Int.	Identification
4286.25	0	FeIII .13(10n)	4347.40	0	FeIII .38(2)	4396.51	00	....
87.54	00	FeIII .61(1)			O II .42(5)	97.68	00	....
88.19	00	FeIII .17(1)	48.14	1	A II .11(20n)	98.50	0	....
		N III .21(-)	48.73	00	....	99.19	00	ClII .14(15)
88.86	0	O II .83(1n)	49.44	3	O II .43(8)	4399.89	00	A II .09(6)
89.58	00	....	50.31	0	FeIII .29(1)	4400.99	0	A II .02(7)
90.55	00	N III .55(-)	51.26	2	O II .27(6)	01.97	00	?P II .97(1n)
91.21	0	FeIII .11(4)	51.98	00	....	03.28	00	FeIII .27(1)
		O II .25(1n)	52.50	1	?FeIII .70(4)	04.01	00	....
92.26	0	O II .23(0n)	53.03	00	....	05.06	0	....
93.29	00	....	53.53	0	O II .60(1n)	05.90	0	....
94.36	0	S II .43(6)	54.49	0	S III .56(2)	06.48	00	FeIII .41(2)
94.80	0	O II .82(3n)	55.48	0	....	07.59	00	....
95.70	00	....	56.52	00	....	08.50	00	....
96.92	0	FeIII .86(10n)	57.23	00	O II .25(0)	09.11	0	....
97.90	00	A II .99(-)			AlIII .24(-)	09.97	1	FeIII .04(3)
4298.96	00	?F II .18(10)	58.53	00	A II .53(1)			C II .06(4)
4300.14	00	....	59.34	00	O II .38(1)	11.12	1	C II .20(5)
00.90	00	....	59.53	00	....	11.47	1	C II .52(5)
01.52	00	FeIII .47(2)	59.80	00	....	12.28	00	Ne I .28(2.5)
03.00	0	O II .81(0d)	60.68	0	....	13.22	00	NeII .20(4,4)
		.06(0d)	61.57	1	S III .53(2)	14.19	0	P II .29(6)
03.86	1	O II .82(5n)	62.33	0	....	14.90	4	O II .91(10)
04.76	0	FeIII .81(10n)	62.75	00	FeIII .68(1)	15.64	00	....
05.29	00	....			Ne I .69(3)	16.25	00	....
07.19	0	AlII .20(3)	63.27	00	FeIII .33(1)	16.96	3	O II .98(8)
08.26	00	....			Ne I .23(0.5)			Ne I .82(4)
08.98	0	O II .96(1n)	64.70	00	S III .73(1)	17.61	00	....
		ClII .06(50)	65.62	0	FeIII .56(3)	18.53	00	FeIII .57(tr)
09.65	00	....	65.92	00	....	19.57	2	FeIII .59(10)
10.28	0	FeIII .37(12n)	66.90	3	O II .90(7)	20.28	00	....
12.07	00	FeIII .13(1)	67.54	00	....	21.02	00	A II .90(7)
		O II .10(0n)	68.12	0	C II .14(4d)	21.62	00	Ne I .56(4)
13.12	00	....			C III .14(-)	22.11	00	....
13.58	00	C II .50(2)	69.26	0	O II .28(4)	23.12	00	....
15.48	00	O II .35(0d, 0d)	69.75	00	FeIII .80(2)	24.06	00	?P II .9 (3d)
					NeII .77(5)	24.96	00	Ne I .80(8)
15.82	00	O II .80(00d)	70.57	00	....	25.57	0	FeIII .48(2)
16.59	00	....	71.46	0	C II .59(3)			Ne I .40(7)
17.18	3	O II .14(8)			A II .36(8)	26.11	1	A II .01(15)
17.95	00	....	72.30	1	C II .49(4)	26.60	00	FeIII .56(tr)
18.62	0	S II .68(4)			Ne I .16(3)	27.25	0	N II .21(2)
19.13	00	....	72.86	0	ClII .91(80)	27.91	0	N II .97(2)
19.67	3	O II .63(8)	73.49	00	....			MgII .00(7)
20.66	00	....	74.30	1	C II .28(5)			Ne I .98(2)
21.10	00	....	75.02	00	N II .00(0)	29.22	0	....
22.40	00	FeIII .45(2)			Ne I .00(0.5)	30.17	0	FeIII .18(1)
24.19	00	....	75.65	00	....			A II .18(9)
24.60	00	....	76.38	00	....	30.98	1	FeIII .95(7)
25.75	1	O II .77(3)	77.88	0	NeII .95(2)			S II .02(1)
		C III .70(8)			Ne I .75(0.5)			A II .02(8)
26.73	00	....	78.34	0	O II .41(0)	31.89	00	FeIII .84(2)
27.42	0	FeIII .41(1)	79.13	00	N III .09(10d)			N II .82(0)
		O II .48(3)	79.64	0	A II .74(8)	32.70	0	N II .74(6n)
28.59	0	O II .62(2)			NeII .50(6)	34.00	00	FeIII .02(2)
30.05	00	....	80.74	00	....			MgII .99(8)
31.01	00	....	81.63	00	....	34.54	00	FeIII .49(1)
31.15	0	O II .13(0d)	82.52	1	....	35.40	00	....
		A II .25(10)	83.36	0	[He I] .24(-)	36.19	00	....
31.87	0	O II .89(2)			?C III .24(1)	37.62	8	He I .55(1)
32.76	1	O II .76(1n)	83.83	00	A II .79(4)	38.24	00	A II .12(1)
		S III .71(4)	84.65	0	MgII .64(8)	38.87	00	....
33.66	00	FeIII .60(3)	85.64	00	....	39.84	0	S III .87(1)
34.83	00	....	86.30	00	....	40.53	00	FeIII .60(3)
36.82	1	FeIII .81(3)	87.26	0	[He I] .30(-)			Ne I .36(2)
		O II .86(6)			.59(-)	41.95	0	N II .99(3n)
37.94	0	....	87.99	30	He I .93(3)	43.09	0	O II .05(5)
38.58	0	SiIII .52(1)	88.73	00	FeIII .65(1)	44.38	00	FeIII .46(1)
39.42	0	....	89.84	00	FeIII .76(1)	47.04	2	N II .03(10)
40.55	80	H .47(H%)	90.56	1	MgII .58(10)	48.23	0	O II .21(6)
41.61	00	....	91.80	00	S II .84(3)	48.94	00	FeIII .97(1)
44.93	0	....	93.55	00	FeIII .52(tr)			A II .88(6)
45.61	2	O II .56(7)	95.88	2	O II .95(7)	49.78	00	FeIII .63(3)
46.53	00	....			FeIII .78(6)	50.36	00	....

TABLE 2 -- Continued

λ	Int.	Identification	λ	Int.	Identification	λ	Int.	Identification
4451.60	0	....	4539.17	0	Ne I .17(4)	4605.59	00	....
52.38	2	O II .38(6)	40.38	0	Ne I .36(10)	07.22	1	FeIII .24(1)
54.27	00	Ne I .28(1)	41.77	0	FeIII .65(4)			N II .15(7)
55.54	00	Ne I .56(2)	44.02	00	FeIII .98(4)	08.28	00	ClIII .21(5)
56.79	00	....			A II .91(1)	09.53	1	A II .60(15)
58.47	00	....	44.21	0	NeII .11(1)			O II .42(4n)
59.09	00	....	45.09	0	A II .08(10)	10.27	0	O II .14(3n)
60.15	00	Ne I .18(6)	46.67	00	....	10.86	00	FeIII .83(1)
61.16	00	....	47.55	00	....	11.82	00	FeIII .80(1)
61.88	00	....	48.43	0	....	12.57	00	FeIII .48(1)
62.71	00	....	49.36	0	....	13.12	00	O II .11(0d)
63.50	00	S II .58(7)	51.12	0	FeIII .15(tr)	13.61	0	O II .67(1d)
64.40	0	S II .42(-)	51.88	0	FeIII .85(tr)			S III .47(00)
65.28	0	....	52.64	5	SiIII .65(9)	13.86	2	N II .87(6)
66.35	0	O II .32(2n)			Ne I .60(3)	15.28	00	....
67.68	0	....	53.83	00	FeIII .77(1)	15.73	00	....
68.53	00	FeIII .51(3)	55.22	00	....	16.42	00	....
69.87	5n	FeIII .92(1)	56.12	00	....	16.87	00	FeIII .95(1)
		[He I] .92(-)	57.82	0	FeIII .82(1)	18.09	00	....
71.56	40	He I .51(6,1)	58.84	00	....	18.83	00	C II .85(5d)
		FeIII .57(4)	60.56	00	....	19.57	0	....
		.16(4)	61.75	00	S II .88(-)	20.42	00	FeIII .39(1)
73.09	0	....	62.70	00	....	21.44	1	N II .39(7)
74.46	00	FeIII .46(3)	63.57	00	FeIII .56(1)			FeIII .39(3)
75.99	00	O II .08(0d)	64.74	00	N II .78(1)	22.35	1	....
77.80	00	N II .74(2)	65.99	00	Ne I .89(4.5)	23.93	00	....
		O II .88(2n)	66.99	00	Ne I .83(3.5)	26.56	00	FeIII .53(1)
79.00	00	....	67.88	5	SiIII .87(7)			P II .61(5)
79.96	2	AlIII .89(3)	69.05	00	FeIII .08(1)	27.29	00	....
		.97(4)			NeII .01(5)	27.91	00	FeIII .94(1)
81.24	5	MgII .33(100)	69.70	0	FeIII .82(4)			NeII .85(3)
		.13(100)	70.97	0	FeIII .85(4)	28.70	00	P II .71(4)
82.42	00	....	72.01	0	ClII .13(100)	30.56	2	N II .54(10)
83.57	00	S II .42(6)	73.26	0	FeIII .14(5)			C II .52(1d)
		FeIII .48(4)	73.78	0	Ne I .76(3)	32.65	0	....
		P II .67(4)	74.80	4	SiIII .78(4)	33.59	0	FeIII .69(2)
84.93	00	....	75.54	00	....	34.91	00	?NeII .73(2)
86.53	00	FeIII .55(1)	76.67	00	....	36.71	00	Ne I .63(5)
		S II .66(3)	77.74	0	....	37.57	0	....
87.70	00	O II .72(0n)	78.39	00	....	38.89	2	O II .85(6)
89.40	0	O II .48(1n)	79.32	0	A II .39(8)	39.78	0	AlII .72(2)
91.22	0	O II .25(3n)	79.94	00	....			.83(1.5)
92.33	00	FeIII .39(3)	80.57	0	....	40.31	0	AlII .36(4)
		S II .3 (00)	81.39	0	....			.38(3.5)
92.60	1	Ne I .69(2)	82.23	00	Ne I .03(7)	41.82	3	O II .81(9)
96.44	00	....			.45(7)			FeIII .90(3)
98.06	00	FeIII .02(tr)	82.93	00	....	43.10	1	N II .09(8)
4499.09	00	?P II .18(7)	83.74	00	....	43.96	00	....
4501.52	00	FeIII .58(2)	84.62	00	....	44.97	0	....
07.74	00	?N II .56(3)	85.32	00	....	45.74	00	FeIII .77(1)
10.91	00	N III .92(6)	86.51	00	....	46.49	00	FeIII .46(2)
12.61	2	AlIII .54(8)	87.36	00	....	47.32	0	C III .40(20)
13.94	00	FeIII .02(1)	87.85	00	P III .91(7)	48.26	00	S II .17(2)
17.47	00	....			P II .91(8)	49.16	4	O II .14(10)
22.08	00	....			A II .90(2)			A II .06(0n)
24.87	00	S II .68(2)	88.99	0	....	50.18	00	C III .16(19)
		.95(6)	90.13	0	....	50.88	2	O II .84(6)
27.70	00	FeIII .67(1)	91.02	2	O II .97(9)	51.60	00	FeIII .57(1)
		Ne I .72(2)	91.69	00	FeIII .84(4)	52.24	00	....
29.15	3	AlIII .18(10)			.35(3)	52.81	00	....
		.91(1)	93.05	00	....	54.27	00	FeIII .19(1)
29.92	00	....	93.86	00	....			SiIV .14(6)
30.44	1	N II .40(5)	94.43	00	....	55.60	00	....
31.67	0	FeIII .59(1)	95.14	00	Ne I .25(4)	56.73	00	S II .74(4)
32.11	00	FeIII .15(1)	96.19	2	O II .17(8)			FeIII .78(2)
32.62	00	....	97.28	0	FeIII .34(2)			SiII .80(-)
33.46	00	FeIII .51(1)	98.09	0	FeIII .98(1)	57.74	00	?A II .94(9)
		S II .3(00)	98.56	00	....	59.00	00	FeIII .00(tr)
34.25	0	MgII .26(4)	4599.38	00	FeIII .27(1)	59.97	00	....
35.15	0	N III .11(2)	4600.49	0	FeIII .43(2)	60.60	00	FeIII .56(tr)
36.56	00	Ne I .31(7)	01.50	2	N II .48(8)	61.64	2	O II .64(9)
37.71	00	Ne I .68(8)	02.21	0	O II .11(2n)	62.47	00	....
		Ne I .75(10)	03.72	00	....	63.12	0	FeIII .21(tr)
		A II .67(4)	04.54	0	....			?AlII .05(0)

TABLE 2 -- Continued

λ	Int.	Identification	λ	Int.	Identification	λ	Int.	Identification
4664.95	00	....	4721.55	00	N II .59(0)	4810.27	0	N II .29(2)
65.69	00	?SiIII .87(0)	22.50	00	....			ClII .06(225)
66.41	00	A II .28(2n)	23.55	00	FeIII .70(2)	11.42	0	ClII .57(12)
67.35	0	FeIII .34(2)	25.28	00	Ne I .14(5)	13.33	0	SiIII .29(2n)
		N II .28(2)	26.92	00	A II .91(10)	15.43	0	S II .52(10)
68.30	00	....	29.74	00	....	16.30	00	....
69.40	0	O II .33(0)	31.96	00	A II .08(5)	17.48	0	Ne I .64(8)
71.10	00	?FeIII .25(tr)	32.86	00	FeIII .70(1)			FeIII .36(1)
71.94	00	....	34.74	00	C II .75(2d)	19.62	1	S II .60(2n,
73.67	1	O II .75(4)	35.83	0	A II .93(15)			2n)
74.73	0	FeIII .79(1)	38.04	00	C II .11(0)			ClII .46(200)
76.25	2	O II .23(8)	40.08	00	....	23.91	00	S II .07(3)
77.01	00	FeIII .24(2)	40.76	00	....			P II .84(0)
		.74(2)	41.63	0	O II .71(3)	25.70	00	....
		O II .00(0)	44.99	0	C II .90(1)	28.95	1	SiIII .92(4n)
78.17	0	Ne I .22(8)	46.29	00	....	30.89	0	....
79.06	00	P II .95(6)	47.48	00	....	35.91	0	S II .85(-)
		Ne I .14(7)	48.17	00	....	36.83	00	ClII .79(20)
79.61	00	....	49.26	00	....	37.79	00	....
80.45	0	Ne I .36(6)	50.36	00	....	38.79	0	....
81.22	00	Ne I .20(4)	51.23	0	O II .34(4)	43.22	0	O II .26(1n)
		?S II .32(00)	52.70	00	Ne I .73(10)	45.10	00	O II .01(1)
82.24	00	A II .29(-)			O II .70(2)	45.85	0	....
		Ne I .15(2.5)	53.52	00	....	47.83	0	A II .90(8)
83.09	00	SiIII .02(2)	54.88	00	?S II .12(2)	48.33	0	....
84.38	00	....	55.53	00	ClII .64(50)	48.98	00	....
85.97	00	....	58.25	00	....	51.88	00	....
87.03	00	....	60.00	00	....	53.41	0	....
87.99	00	....	61.24	00	....	56.68	0	O II .49(2)
89.24	00	....	63.42	00	S II .38(1)			.76(2)
89.85	00	FeIII .87(tr)	64.53	00	....	57.06	00	ClII .04(10)
91.68	0	FeIII .63(1)	64.99	0	A II .89(10)			FeIII .06(tr)
		O II .47(1)	66.45	00	....	58.11	00	....
93.13	00	....	68.07	0	....	59.77	0	....
94.76	0	FeIII .57(4)	69.29	00	....	61.28	80	H .33(Hβ)
96.05	0	N II .91(1)	70.92	00	ClII .09(40)	62.74	0	FeIII .66(-)
96.45	00	O II .36(2)	73.94	00	N II .22(2)	64.33	00	Ne I .35(3)
97.68	0	FeIII .69(1)	75.17	00	....			P II .38(4)
4699.18	1	O II .21(7,7)	79.74	0	N II .71(4)	71.72	0	O II .58(3)
		FeIII .22(1)	80.94	00	Ne I .88(3)			FeIII .86(2)
4701.04	0	O II .23(2)	81.79	00	ClII .82(50)	80.02	0	A II .90(12)
03.10	0	O II .18(3)	83.42	00	....	82.11	00	A II .25(-)
04.26	00	Ne I .40(15)	84.35	00	....	83.41	0	....
		N II .33(0)	85.34	0	ClII .44(50)	85.70	0	S II .63(-)
05.40	2	O II .36(8)	86.32	00	....	4890.85	0	O II .93(4)
06.92	00	....	87.25	0	....	4902.45	1	....
08.02	0	....	88.05	0	N II .13(5)	04.55	0	A II .75(6)
08.75	00	Ne I .85(12)	88.93	0	Ne I .93(12)			ClII .76(135)
09.90	1	Ne I .06(10)	91.10	00	....	05.85	0	....
		O II .04(5)	91.95	00	ClII .04(12)	06.89	1	O II .88(5)
10.92	00	....			S II .02(3)			SiII .88(-)
11.99	0	FeIII .98(1)	93.18	0	....	09.15	00	....
		Ne I .06(10)	94.72	00	ClII .54(250)	10.66	0	[He I] .75(-)
13.23	10	He I .20(3,1)	96.85	0	....	14.20	0	ClII .32(12)
15.37	00	Ne I .34(15)	98.29	00	ClII .40(15)	16.27	00	....
16.64	1	SiIII .66(-)	4799.43	0	....	17.10	0	S II .15(7)
17.61	00	....	4800.69	0	....	17.77	00	ClII .72(125)
18.41	00	N II .43(2)	02.63	0	S III .81(-)	19.36	0	....
19.22	00	FeIII .12(2)	03.27	1n	N II .27(6)	19.96	00	....
		?NeII .37(1.5)	05.92	1	A II .07(20)	20.52	1	[He I] .35(-)
20.21	00	P II .26(3)	07.20	0	....	4922.02	10	He I .93(-)
			09.21	00	....			

two stages of ionization contribute lines. A survey of the *O* II lines shows that, when the excitation potential is higher than about 28 volts, only the strongest lines appear. Although for some elements lines of excitation potential greater than 30 volts have been identified, it is not felt that much weight should be given to these identifications because the general level of excitation is considerably lower than this.

When the wave-length coincidences had been found, the identifications were checked by an attempt to establish full multiplets. For this work Part I of the "Revised Multiplet Table"[5] was invaluable. If a series of reasonably full multiplets with estimated stellar intensities closely paralleling the laboratory intensities could be established for an element, the proposed identification was retained; if not, it was rejected. Additional lines of *Ne* I were identified from the wave lengths given by Meggers and Humphreys[6] (interferometer measures) and by Paschen.[7] A number of unclassified *Fe* III lines were identified from an unpublished list very kindly loaned to the writer by Mrs. Sitterly. In this manner about 70 per cent of the 877 lines measured were identified.

Use of the *M.I.T. Tables*[8] suggested *Rb* II, *Kr* II, and *Th* III as sources of the unidentified lines; but the multiplet structure of these spectra could not be adequately established in γ Pegasi; hence all coincidences found were considered as random and were disregarded. The lack of knowledge of the third and fourth spectra of the metals *Ti*, *V*, *Cr*, *Mn*, and *Ni* in the photographic region is to be deplored, as it would probably lead to the identification of many faint lines.

On the average, less than one and one-half lines per angstrom were measured. Since the reality of each feature was checked by visual inspection of all the plates, it is felt that the number of spurious lines and of random coincidences is low. The reality of many of the weak unidentified lines is supported by the fact that Kühlborn,[3] in most cases, gives practically identical wave lengths and intensities.

The elements for whose spectra comprehensive lists of lines in the region λλ 3965–4935 could be found are summarized in Table 3. The first four columns are self-explanatory. The abundances in the earth are taken from Von Klüber.[9] In column 5 "Yes" means that the spectrum is definitely present in γ Pegasi, most of the possible multiplets being represented; a question mark (?) means that the identifications are not too good but that the spectrum is probably present; (??) mean that some coincidences have been found suggesting this spectrum but that it is probably not present; "No" means that it is not present. The figures in column 6 refer to notes at the end of the table.

In general, it seems that all elements with the proper ionization and excitation potential will be found if they have lines in the region under consideration and if their abundance in the earth is reasonably high. The only exception of note is potassium. This element is very abundant in the earth, and the *K* II spectrum has many strong lines of favorable wave length and excitation potential for appearance in the spectrum of γ Pegasi. However, not one line could be identified with certainty; in fact, there was nothing at all where most of the strong lines should be. This result is in agreement with that obtained by Struve,[2] but contrary to that of Kühlborn.[3]

II. A STUDY OF THE *He* I LINES

PERMITTED LINES

A review of the material in Table 2 shows small redward displacements for the lines of the diffuse and sharp series of *He* I and a violet displacement for λ 3965, which is the only member of the principal series observed. Similar displacements have been observed in τ Scorpii by Adams and Merrill[10] from measurements on coudé plates.

[6] *J. Research Nat. Bur. Standards*, **13**, 293, 1934. [7] *Ann. d. Phys.*, **60**, 405, 1919.

[8] *M.I.T. Wavelength Tables* (New York: Technology Press, John Wiley & Sons, Inc., 1939).

[9] *Das Vorkommen der chemischen Elemente im Kosmos* (Leipzig: Johann Ambrosius Barth, 1931), p. 29.

[10] *Ap. J.*, **97**, 98, 1943.

The theory of Stark effect for constant electric fields has been developed by Foster[11] and investigated by him in the laboratory. According to theory and experiment, the *He* I lines are displaced, the amount and direction of the displacement depending on the field strength and the levels between which the line arises. In stellar atmospheres the electric field is caused by random encounters of the helium atoms with charged particles. Thus only qualitative agreement of stellar displacements with those predicted by con-

TABLE 3

SPECTRA IDENTIFIED IN γ PEGASI

Element (1)	Abundance in Earth (2)	Spectrum (3)	I.P. (Volts) (4)	Spectrum Found (5)	Remarks (6)	Element (1)	Abundance in Earth (2)	Spectrum (3)	I.P. (Volts) (4)	Spectrum Found (5)	Remarks (6)
H	8.8×10^{-3}	I	13.54	Yes		*Si*	2.6×10^{-1}	I	8.11	No	2
								II	16.27	Yes	
He	4.2×10^{-9}	I	24.48	Yes				III	33.32	Yes	
		II	54.17	No	1			IV	44.95	Yes	
Li	5.0×10^{-5}	I	5.37	No	2	*P*	1.2×10^{-3}	I	10.9	No	2
		II	75.31	No	1			II	19.57	?	8
								III	30.03	Yes	
Be	5.0×10^{-6}	I	9.28	No	2						
		II	18.13	No	3	*S*	4.8×10^{-4}	I	10.31	No	2
								II	23.3	Yes	
B	1.4×10^{-5}	I	8.26	No	2			III	34.9	Yes	
		II	25.02	??	4						
		III	37.77	??	5	*Cl*	1.9×10^{-3}	I	12.95	No	2
								II	23.70	Yes	
C	8.7×10^{-4}	I	11.20	No	2			III	39.69	?	8
		II	24.28	Yes							
		III	47.67	Yes		*A*	3.6×10^{-6}	I	15.69	No	2
								II	27.76	Yes	
N	3.0×10^{-4}	I	14.49	No	2			III	40.75	No	1
		II	29.49	Yes							
		III	47.24	??	5	*K*	2.4×10^{-2}	I	4.32	No	2
								II	31.7	No	9
O	1.9×10^{-1}	I	13.56	No	2						
		II	35.00	Yes		*Ca*	3.4×10^{-2}	I	6.09	No	2
		III	54.71	??	5			II	11.82	Yes	10
								III	51.00	??	11
F	2.4×10^{-4}	I	17.35	No	2						
		II	34.84	Yes		*Sc*	7.5×10^{-7}	I	6.7	No	2
								II	12.8	No	2
Ne	5.0×10^{-9}	I	21.47	Yes				III	24.61	??	3
		II	40.91	?	5						
						Fe	4.7×10^{-2}	I	7.86	No	2
Na	2.6×10^{-2}	I	5.12	No	2			II	16.16	No	2
		II	47.10	?	6			III	30.48	Yes	
Mg	1.9×10^{-2}	I	7.61	No	2	*Rb*	3.4×10^{-5}	I	4.16	No	2
		II	14.97	Yes				II	27.36	??	8, 3
Al	7.5×10^{-2}	I	5.96	No	2	*Kr*	2.0×10^{-10}	I	13.93	No	2
		II	18.75	?	7			II	26.4	??	8, 3
		III	28.33	Yes							
						Th	2.5×10^{-5}	III	29.5	??	8, 3

NOTES TO TABLE 3

1. The excitation potential is too high for this spectrum to appear.
2. The ionization potential is too low for this spectrum to appear.
3. The terrestrial abundance is low.
4. Only one line is possible, λ 4191.95, and it would be blended with *Fe* III.
5. A few coincidences were found, but the excitation potential is rather high.
6. Two out of three possible coincidences found, but the excitation potential is rather high.
7. A good many coincidences found, but the ionization potential is rather low.
8. Quite a few coincidences were found, but the multiplet structure could not be adequately established in the star.
9. The absence of this element cannot be attributed to unfavorable excitation potential or unfavorable wave length of the strong lines.
10. Only the H line is measured.
11. Only one line of rather high excitation potential occurs in the region under study, giving a poor coincidence with a stellar line.

[11] *Proc. R. Soc., London, A*, **117**, 137, 1927.

stant field-strength theory is to be expected. M. K. Krogdahl[12] gives theoretical results for the broadening and displacement of the *He* I lines in the case of a fluctuating field.

Data on the observed and theoretical displacements are given in Table 4. Column 3 gives the observed displacements $\lambda_{star} - \lambda_{lab}$ for γ Pegasi and column 4 those for τ Scorpii, measured by Adams and Merrill. For the triplet lines I have chosen a mean wave length, weighted according to the statistical weights of the two components. Adams and Merrill use the wave length of the strongest component alone. In order to compare results, Adams and Merrill's displacements have been adjusted to my system of wave lengths for the triplet lines. Column 5 gives the mean displacement calculated by Foster for a constant field of 10 kv/cm, the lowest field strength for which Foster calculates displacements. A field strength of 1–10 kv/cm is suggested[13,14] by the relative strengths of the

TABLE 4

DISPLACEMENTS OF *He* I LINES $\lambda_{STAR} - \lambda_{LAB}$

Transition	λ	Observed*		Theoretical	
		γ Peg	τ Sco	Foster 10 Kv/Cm	Krogdahl (For τ Sco)
(1)	(2)	(3)	(4)	(5)	(6)
2^3P-4^3D	4471	+0.05 A	−0.02 A	+0.22 A	+0.04 A
2^3P-5^3D	4026	+ .02	+ .00	+ .87	+ .12
2^1P-4^1D	4921	+ .09	.....	+ .42	+ .07
2^1P-5^1D	4388	+ .06	+ .04	+1.29	+ .28
2^1P-6^1D	4144	+ .10	+ .07	.....	.....
2^1P-7^1D	4009	+ .04	+ .05	.....	.....
2^3P-4^3S	4713	+ .03	− .02	+ .01	+ .005
2^3P-5^3S	4121	+ .04	− .02	+ .06	+ .011
2^1P-5^1S	4437	+ .07	+ .02	+ .04	.....
2^1P-6^1S	4169	+ .13	.....	.....	.....
2^1P-7^1S	4024	+ .05	.....	.....	.....
2^1S-4^1P	3965	−0.09	−0.02	−0.08	−0.017

* Weighted mean laboratory wave length used for the triplets. If the wave length of the strongest component is used, the displacements for λ 4471, λ 4026 should be increased by +0.03 A, that for λ 4713 by +0.06 A, and that for λ 4121 by +0.04 A.

forbidden lines. Column 6 gives the mean displacements calculated by M. K. Krogdahl[15] according to the fluctuating-field collisional theory for the lines in τ Scorpii.

Only the diffuse-series lines are displaced enough by low electric fields for a comparison of theory and observation to yield significant results. The data of Table 4 show that the displacements of the *He* I lines are small and not of the order of magnitude predicted and found experimentally for a constant field of 10 kv/cm. If we adopt the mean field in stars as 5 kv/cm,[13,14] interpolation from the graphs in Foster's paper[11] (Pls. 7–13) would suggest displacements only half those quoted in Table 4, but still there is no agreement with observation. The displacements calculated by M. K. Krogdahl for the diffuse-series lines seem more nearly in agreement with observation; however, the displacements observed for 2^3P-5^3D (λ 4026) and 2^1P-5^1D (λ 4388) are significantly less than the predicted values; for, since the lines are strong and sharp, the accidental error of measurement is less than ±0.01 A. The results from the triplet lines should be given low weight because of the uncertainty of what to use for the "laboratory wave length." The smallness of

[12] *Ap. J.*, **100**, 333, 1944; **102**, 64, 1945; **105**, 327, 1947.

[13] Struve, *Ap. J.*, **70**, 90, 1929.

[14] Goldberg, *Ap. J.*, **89**, 623, 1939.

[15] *Ap. J.*, **105**, 327, 1947.

the observed displacements of λ 4026 and λ 4388 may be partly due to the blending effect of the forbidden lines which occur to the violet. For the principal and sharp series lines the smallness of the predicted and observed displacements makes it difficult to decide whether the agreement between theory and observation is significant or merely fortuitous. One possible additional factor not included in either theory of the displacements is the effect of stratification, particularly for the diffuse-series lines. Since these lines are very strong, the cores are formed at the top of the atmosphere in regions of low density, whereas the forbidden lines are formed and the shifts occur at lower, more dense levels. Since the cores of the *He* I lines are measured, the observed shifts might be expected to be less than those predicted. This effect would not be so important for the principal and sharp series lines, since they are fairly weak.

FORBIDDEN LINES

The probability of the occurrence of a forbidden transition ($\Delta l = 0, 2, 3$) depends upon the strength of the electric field. Foster[11] has calculated the intensities of the forbidden components for various field strengths for some lines. Table 5, derived from the

TABLE 5

THEORETICAL RELATIVE STRENGTHS OF *He* I LINES

TRANSITION	TRIPLETS			SINGLETS		
(1)	λ (2)	10 Kv/Cm (3)	40 Kv/Cm (4)	λ (5)	10 Kv/Cm (6)	40 Kv/Cm (7)
2P−4D	4471.5	10	10	4921.9	10	10
2P−4F	4469.9	1.4	6	4920.4	2	4
2P−4P	4517.4	00	0	4910.7	0	1.6
2P−5D	4026.2	10	10	4387.9	10	10
2P−5F	4025.5	7	14	4387.6	6	4
2P−5G	4025.4	4	12	4387.3	2.4	1
2P−5P	4045.2	0	2	4383.2	1.5	7.5

results of his calculations at fields of 10 and 40 kv/cm, gives a guide to the expected relative strengths of the forbidden lines in main-sequence B stars. The strengths of the forbidden lines are expressed in terms of that of the permitted line, which has been arbitrarily put equal to 10. Since, theoretically, the sum of the strengths of all the component lines must be constant, the strength of the permitted line decreases as the field increases, to allow for the increasing strengths of the forbidden lines. In stars, however, owing to the saturation of the permitted lines, the strengths of the permitted lines will probably remain more or less the same with increasing field, whereas the forbidden lines will increase in strength in the manner indicated in Table 5. In comparing forbidden lines with permitted lines, it should be remembered that a forbidden line is intrinsically deeper than a permitted line;[16] hence the same apparent strength can be obtained with fewer active atoms. Qualitative agreement with the intensities in Table 5 (cols. 3 and 6) is expected.

Although fields of less than 10 kv/cm are expected in stars, the inclusion of the values for fields of 40 kv/cm in Table 5 brings out some interesting points. Because of the weakness of the 2^3P-m^3P transitions it seems unlikely that these lines will occur in stellar

[16] *Ap. J.*, **104**, 327, 1946.

spectra. The 2^1P-m^1P lines have greater relative strength and might possibly be seen. Secondly, the 2^3P-m^3F and 2^3P-m^3G lines appear to be much more sensitive to field strength than are the corresponding singlet lines. If this effect were pronounced enough, it could introduce a luminosity effect between intermediate and dwarf B-type stars. Since the dwarf stars have denser atmospheres, the average electric field will be greater, thus the observed line at λ 4026, which is a blend on most dispersions of 2^3P-5^3D, 2^3P-5^3F, and 2^3P-5^3G, will be strengthened, whereas the line λ 4388, which is a blend of 2^1P-5^1D, 2^1P-5^1F, and 2^1P-5^1G, will remain much the same as in a star of intermediate luminosity.

Since the forbidden lines are rather weak and diffuse, a comparison of the observed displacements with those calculated by Foster or by M. K. Krogdahl is not very significant. The relatively strong forbidden lines 2^3P-4^3F λ 4469.92; 2^3P-5^3F, 2^3P-5^3G λ 4025.49, λ 4025.40; 2^1P-4^1F λ 4920.35; 2^1P-5^1F, 2^1P-5^1G λ 4387.59, λ 4387.30, have been measured near their theoretical zero-field positions. Weak lines have been found close to the zero-field positions of 2^1P-6^1F λ 4143.44, 2^1P-4^1P λ 4910.75, 2^1P-5^1P λ 4383.24, 2^1P-6^1P λ 4141.34, 2^1P-7^1P λ 4007.81. A search was made for the lines 2^3P-4^3P λ 4517.43 and 2^3P-5^3P λ 4045.16. There is a faint line at λ 4517.45; but, in view of the intensity relations in Table 5, it seems unlikely that this line is [*He* I]. No line attributable to [*He* I] could be found at λ 4045.16.

The luminosity effect predicted in λ 4026 is indicated by equivalent widths derived from high-dispersion plates. Measurements of good internal consistency are provided by my measurements[17] of the equivalent widths of *He* I lines from high-dispersion plates taken at the Dominion Astrophysical Observatory, and by Unsöld's[18] measurements in the spectrum of τ Scorpii. The latter used coudé plates taken at the McDonald Observatory. Comparison of the strength of λ 4026 to that of the other *He* I lines for η Ursae Majoris and τ Scorpii, which are in luminosity class V (dwarfs) on the system of the Yerkes spectral atlas,[1] shows that λ 4026 is significantly stronger than any other *He* I line in the spectrum. In the intermediate stars, γ Pegasi and ι Herculis, class IV, λ 4026 is about the same strength as λ 4471. It does not seem possible to explain the increased relative strength of λ 4026 in the dwarf stars by blends with lines of other elements. An exact explanation of the strengths of the helium lines in dwarf and giant stars requires the solution of the problem of radiative transfer complicated by Stark effect. In the case of λ 4026 the blending of the near-by forbidden lines will likely contribute to the observed line strength; and, since these lines are quite sensitive to field strength, it is possible that they may be significant in producing the final observed equivalent width. It is doubtful whether the luminosity effect mentioned here is pronounced enough to be useful on low-dispersion plates.

I am indebted to Dr. Otto Struve for suggesting this problem and for his constant advice on the problems involved in the study of a B star; and to Dr. W. A. Hiltner, who very kindly loaned the excellent plates of γ Pegasi used. My special thanks are due to Dr. J. L. Greenstein, whose criticism and advice have been invaluable. Dr. W. S. Adams very kindly lent me some coudé spectrograms of γ Pegasi in the λ 4900 region taken by H. W. Babcock at the Mount Wilson Observatory.

[17] *J.R.A.S. Canada*, **38**, 385, 1944. [18] *Zs. f. Ap.*, **21**, 22, 1941.

THE INTENSITIES AND PROFILES OF LINES IN SOME B-TYPE STARS*

ANNE B. UNDERHILL†
Yerkes and McDonald Observatories
Received February 24, 1948

ABSTRACT

The equivalent widths and central absorptions of $H\gamma$, $H\delta$, the *He* I lines λλ 4471, 4026, 4388, 4144, 4009; the *Mg* II line λ 4481; the *Si* II lines λ 4128, λ 4130; and the *Si* III lines λλ 4552, 4568, 4574 have been found from McDonald coudé plates for the B-type supergiants ρ Leo, χ^2 Ori, o^2 CMa, χ Aur, η CMa, and β Ori, and for the less luminous stars ϵ CMa, γ Peg, τ Her, and ζ Dra. The central absorptions are corrected for instrumental distortion. Profiles of $H\gamma$ are given for all the stars studied. Profiles of the other lines are given only for o^2 CMa, ϵ CMa, and γ Peg.

The interpretation of the hydrogen-line profiles is discussed, and model atmospheres with $\theta_0 = 0.30$ and $\log g = 2.00$ and 4.09 are calculated. The line intensities predicted from these models are compared with the observed intensities in o^2 CMa, and γ Peg; and it is shown how such models can be used to derive relative abundances of the elements and the shape of the line-absorption coefficient. The line-absorption coefficient is found to have a Doppler half-width $\Delta\lambda_D$ of 37 ± 2 km/sec in the supergiant o^2 CMa, and 27 ± 2 km/sec in the giant ϵ CMa.

The strength and shape of the absorption lines in a stellar spectrum reflect the physical properties of the stellar atmosphere. For this reason line profiles are an additional important source of information about conditions in the stellar atmosphere. The purpose of this investigation is to obtain profiles of some of the strongest lines in B-type stars and to show how they may be interpreted. The profile of a stellar absorption line obtained from a microphotometer tracing of the spectrum is distorted by the spectrograph. However, it turns out that for lines which are broad compared to the instrumental profile the correction to the measured central absorption is small; hence the true central absorption of the line can be determined quite accurately with only a relatively crude method of correction. Inspection of high-dispersion coudé plates of B-type stars shows that most of the strong lines are broad; thus the instrumental correction will be small for these lines, and the profiles obtained will be very similar to the true profiles.

1. *Procedure.*—Table 1 lists the stars studied and the plates used. The spectral type and luminosity class are according to unpublished work of W. W. Morgan. The star ζ Dra is peculiar in some respects,[1] and at present there is no luminosity classification for it, other than the statement that it is not a high-luminosity star. The estimated rotation classes ("Rot.") for the stars are according to Struve.[2] An effort has been made to select only stars with zero or low rotation, though the list of objects studied has been influenced by the coudé plates available. The range of spectral type from B8 to B1 is well covered in the supergiants and more sketchily for the stars of lower luminosity. The serial numbers of the plates used are tabulated with a symbol indicating the type of calibration used: "T" means the tube sensitometer of the McDonald Observatory, "W" means a linear wedge calibration. I am indebted to Dr. Jesse L. Greenstein for the use of Cd96, 126, 134, 255, 263, 680, 684, 689, 690, 691, 719, 720, 721; and to Dr. W. A. Hiltner for Cd461, 481, 555. The remaining plates I took myself at the McDonald Observatory.

* *Contributions from the McDonald Observatory, University of Texas*, No. 149.

† This work was completed during tenure of a scholarship from the Canadian Federation of University Women.

[1] Morgan, Keenan, and Kellman, *An Atlas of Stellar Spectra* (Chicago: University of Chicago Press, 1943), p. 12.

[2] *Ap. J.*, **74**, 225, 1931.

The lines chosen are those which are strong over the whole spectral range studied and which appear in the limited wave-length range of the available plates. They are, for hydrogen, $H\gamma$ and $H\delta$; for *He* I the triplet diffuse-series lines λ 4471, λ 4026, and the singlet diffuse-series lines λλ 4388, 4144, 4009; for *Mg* II λ 4481; for *Si* II λ 4130, λ 4128; and for *Si* III λλ 4574, 4568, 4552. The *Si* II lines and *Si* III lines appear equally strong at about B3; for later types, only *Si* II is measured and for earlier types only *Si* III.

All the plates were taken with the coudé spectrograph of the McDonald Observatory on Eastman 103*a*-O emulsion and were calibrated according to the system in use when they were obtained. The McDonald coudé spectrograph and the wedge-slit method of calibration are described by Hiltner and Williams.[3] The dispersion is about 3.2 A/mm at $H\gamma$. From plates on which two methods of calibration were used it was found that the same calibration-curve is obtained with the tube sensitometer as with the wedge slit, though the latter method of calibration is to be preferred. From the wedge-slit calibration it can be shown that over the wave-length range used, λλ 4000–4600, the

TABLE 1

STARS STUDIED

Star	Type	Rot.	Plates Used
ρ Leo	B1 Ib	3	Cd255(T), 263(T)
χ^2 Ori	B2 Ia	1	Cd680(T,W), 734(W), 738(W)
o^2 CMa	B3 Ia	1	Cd691(T,W), 728(W)
χ Aur	B3 Ib	0	Cd684(T,W)
η CMa	B5 Ia	.....	Cd96(T), 126(T), 134(T), 719(T,W), 720(T,W), 730(W)
β Ori	B8 Ia	0	Cd481(W), 721(T,W)
ϵ CMa	B2 II	1	Cd689(T,W), 690(T,W), 729(W)
γ Peg	B2.5 IV	0	Cd461(W), 555(W)
τ Her	B5 IV	0	Cd733(W), 740(W)
ζ Dra	B8 ...	0	Cd737(W)

calibration-curve is essentially the same for all wave lengths. Only plates of good density for photometric work were used, so that the densities fell on the linear part of the calibration-curve except in a few cases for the cores of the strongest lines. Since the transmission of the coudé spectrograph for light of wave length less than 4100 A decreases rapidly, a number of plates which were of usable density at λ 4300 were too thin for the accurate determination of the profiles of $H\delta$, λ 4026 and λ 4009. The measures given for these lines are only from plates of good density in these regions. The Yerkes microphotometer was used with both amplifying systems, the new circuit[4] being used for thin plates.

Some of the microphotometer tracings were reduced to intensities by means of the semi-automatic recording intensitometer of the Dominion Astrophysical Observatory, Victoria, B.C. I am grateful to Dr. J. A. Pearce for the privilege of using this instrument, thus speeding the tedious job of reducing all the microphotometer tracings to intensities point by point. No systematic differences were found between the profiles derived from the intensitometer tracings and those obtained in the conventional manner.

To correct for the instrumental broadening, the following integral equation must be solved:

$$f(x) = \int_{-\infty}^{+\infty} f'(x-y)\, g(y)\, dy\,, \qquad (1)$$

[3] *Photometric Atlas of Stellar Spectra* (Ann Arbor: University of Michigan Press, 1946), Book I.

[4] *Pub. A.S.P.*, 58, 373, 1946.

where $f(x)$ is the measured intensity distribution in a spectral line, $g(y)$ is the true intensity distribution in the line, and $f'(x-y)$ is the instrumental profile. The problem is to obtain $g(y)$, knowing $f(x)$ and $f'(x-y)$. Van de Hulst and Reesinck[5] discuss this problem and give a method of solution, using Voigt functions. The present semi-empirical method, which is based on the well-known half-breadth method, was worked out before the more elegant method of van de Hulst and Reesinck came to the notice of the writer. Tests of the two methods show that they yield similar results. For the lines under discussion the simpler method used is sufficiently accurate.

If we can assume that

$$g(y) = A_c e^{-(y/a)^2}, \tag{2}$$

where A_c is the true central absorption of the line and a is the half half-width of the line, and if we assume that the instrumental profile is given by

$$f'(x-y) = \frac{1}{b\sqrt{\pi}} e^{-(x-y)^2/b^2}, \tag{3}$$

where b is the half half-width of the instrumental profile, we find from equation (1) that

$$\frac{1}{A_c^2} = \frac{1}{A_m^2} - \frac{\pi b}{W}. \tag{4}$$

Here A_m is $f(0)$, the measured central absorption of the line, and W is the equivalent width of the line. We have

$$W = \sqrt{\pi}\, a A_c. \tag{5}$$

From equation (4) we see that, if we know b, we can obtain the true central absorption of a line from measurement of its apparent central absorption and its equivalent width. For strong lines, $W \gg b$, the correction is negligible. Since the moderately strong lines in B-type stars are closely Gaussian in apparent form (as can be seen from the profiles of Figure 4 by plotting $\log A/A_c$ against Δx^2, where Δx is the distance from the center of the line), the assumption expressed in equation (2) is valid. If we can find a b such that equation (3) represents the instrumental profile reasonably well, equation (4) can be used to obtain corrected central absorptions of the lines. This correction will be small so long as $1/A_m^2$ is large with respect to the term containing W. For the lines in B-type stars this is nearly always the case on coudé dispersion. Since the correction is small, it does not have to be critically determined, and the relatively crude method outlined is sufficient.

The half half-width, b, of the instrumental profile was determined empirically in the following manner. Microphotometer tracings were made of several sharp lines in the iron-arc comparison spectrum on the spectrogram, and a mean profile was derived. This was called the "instrumental profile" and is identical with that given by Hiltner and Williams.[3] Actually, the iron-arc lines used are not infinitely sharp, but they are sufficiently so for our purpose. The instrumental profile has somewhat broader wings than a Gaussian profile with the same half-width and central intensity would have. To find a half half-width that would reproduce the effect of this profile, equation (1) was solved graphically for $f(0)$, which is A_m, when an arbitrary $g(y) = A_c e^{-(y/a)^2}$ was used with the observed instrumental profile $f'(x-y)$. Then equation (1) was solved with the same $g(y)$ but with $f'(x-y)$ given by equation (3) and the constant b was adjusted until the same $f(0)$ was obtained. The constant b thus determined is the effective half half-width of the instrumental profile. The arbitrary constants A_c and a in the expression for $g(y)$ were given a series of values such that line profiles typical of B stars resulted. The effec-

[5] *Ap. J.*, 106, 121, 1947.

TABLE 2

Equivalent Widths and Central Absorptions

Star	Wt.	W	A_m	A_c	Wt.	W	A_m	A_c	Wt.	W	A_m	A_c
	$H\gamma$				$H\delta$				He I λ 4471			
ρ Leo	2	2.276	50	50	1	1.543	46	46	2	0.953	43	43
χ^2 Ori	2.5	1.601	51	51	1	1.148	40	40	2.5	0.905	46	47
o^2 CMa	1.5	1.818	53	54	1	1.351	44	44	1.5	0.906	50	51
χ Aur	1	1.458	42	42	.....	.....	.....	.....	1	0.560	34	35
η CMa	4	1.597	49	49	3	1.606	53	54	3	0.781	50	51
β Ori	2	1.526	52	53	2	1.767	61	61	2	0.395	34	35
ε CMa	3	2.546	54	54	3	2.290	49	49	3	0.941	50	51
γ Peg	2	4.002	62	62	2	5.113	62	62	2	1.222*	57	58
τ Her	2	7.520	70	70	.....	.....	.....	.....	2	1.014†	46	46
ζ Dra	1	8.623	77	77	1	9.315	86	86	1	0.671‡	32	32
	He I λ 4026				He I λ 4388				He I λ 4144			
ρ Leo	1	0.704	38	39	2	0.398	26	26	2	0.364	24	24
χ^2 Ori	.....	.....	.....	.....	2.5	.607	37	37	2.5	.307	23	24
o^2 CMa	1	0.597	50	50	1.5	.494	33	34	1.5	.376	30	30
χ Aur	.....	.....	.....	.....	1	.437	31	32	1	.275	23	23
η CMa	4	0.547	42	42	3	.439	32	32	4	.346	29	30
β Ori	1	0.397	32	32	2	.249	22	23	2	.153	19	20
ε CMa	3	0.884	45	45	3	.605	39	39	3	.447	32	32
γ Peg	1	1.311§	54	54	2	.767	50	50	2	.658	44	44
τ Her	.....	.....	.....	.....	1	.428	24	24	2	.412	23	23
ζ Dra	1	0.760	43	43	1	0.295	18	18	1	0.210	19	19
	He I λ 4009				Si II λ 4130				Si II λ 4128			
ρ Leo	1	0.262	18	18	.....	.....	.....	.....	.....	.....	.....	.....
χ^2 Ori	.....	.....	.....	.....	.....	.....	.....	.....	.....	.....	.....	.....
o^2 CMa	.....	.....	.....	.....	1.5	0.196	16	16	1.5	0.174	16	16
χ Aur	.....	.....	.....	.....	1	.143	15	15	1	.164	16	16
η CMa	4	.264	24	24	4	.237	23	24	4	.238	25	26
β Ori	1	.165	16	16	2	.252	27	28	2	.253	27	27
ε CMa	3	.405	27	27	1	.076	13	14	1	.056	9	10
γ Peg	1	.640	32	32	2	.030	13	20	2	.031	14	22
τ Her	.....	.....	.....	.....	2	.211	24	24	2	.166	19	20
ζ Dra	1	0.221	13	13	1	0.249	24	24	1	0.225	25	25
	Si III λ 4574				Si III λ 4568				Si III λ 4552			
ρ Leo	2	0.310	22	22	1	0.461	29	30	2	0.594	35	36
χ^2 Ori	2.5	.231	19	20	2.5	.396	29	29	2.5	.522	34	34
o^2 CMa	1	.176	12	13	1.5	.256	19	19	1.5	.300	22	23
χ Aur	1	.075	9	10	1	.136	13	14	1	.159	15	16
η CMa	2	.099	10	10	2	.156	14	15	2	.198	18	19
β Ori	.....	.....	.....	.....	.....	.....	.....	.....	.....	.....	.....	.....
ε CMa	2	.254	26	27	3	.346	36	38	3	.418	41	43
γ Peg	2	0.088	23	.....	2	0.112	32	.....	1	0.162	38	.....
τ Her	.....	.....	.....	.....	.....	.....	.....	.....	.....	.....	.....	.....
ζ Dra	.....	.....	.....	.....	.....	.....	.....	.....	.....	.....	.....	.....

* The equivalent width of λ 4471 only is 0.911 A; of λ 4470 it is 0.311 A.

† The equivalent width of λ4471 only is 0.776A; of λ4470 it is 0.238A.

‡ The equivalent width of λ 4471 only is 0.486 A; of λ 4470 it is 0.185 A.

§ The equivalent width of λ 4026 + [*He* I] only is 0.947 A.

TABLE 2—*Continued*

Star	Wt.	W	A_m	A_c	Star	Wt.	W	A_m	A_c
	Mg II λ 4481					*Mg* II λ 4481			
ρ Leo	2	0.252	15	15	β Ori	2	0.490	43	45
χ^2 Ori	2.5	.241	19	19	ε CMa	3	.223	26	27
o^2 CMa	1.5	.415	32	33	γ Peg	2	.172	38	.....
χ Aur	1	.370	26	27	τ Her	2	.370	38	39
η CMa	4	0.511	39	40	ζ Dra	1	0.428	38	39

tive b is that value which gave the best representation of the blurring effects of the true instrumental profile on all these lines. As a final check, arbitrary wings such as might occur for strong lines were drawn on $g(y)$, and the integration of equation (1) was performed graphically for $f(0)$ when the actual $f'(x - y)$ was used and when a Gaussian $f'(x - y)$ with the half half-width determined above was used. These two integrals agreed satisfactorily.

With the half half-width, b, thus determined, a family of curves giving A_c as a function of W was plotted from equation (4), for a series of values of A_m. The observed A_m's were corrected to A_c's by interpolation in this graph. To avoid the difficulties of the changing dispersion, it is convenient to express b and W as millimeters on the tracing. An example of the order of magnitude of the instrumental correction may be of interest. For tracings magnified thirty times from the plate, $b = 1.26$ mm. A typical weak line is λ 4128 in ε CMa on Cd729. For this line $W = 0.72$ mm; $A_m = 9$ per cent. From the graph we estimate $A_c = 10$ per cent. From equation (4), $A_c = 9.2$ per cent. The correction is smaller than the probable error of measurement. Only the *Mg* II line and the *Si* III lines in γ Peg are so narrow and sharp that the corrections are very large and uncertain. For these lines the correction obtained is very sensitive to the shape of the apparent profile. Since the apparent profile cannot be determined accurately enough, the central absorptions of these lines are not corrected. The central absorptions of all the other lines have been corrected by the graphical method described.

2. *Observed line intensities and central absorptions.*—The measured equivalent widths and central absorptions are given in Table 2. Weights are assigned according to the number of plates used in the determination. A few of the plates which are weak or streaked by poor guiding are given half-weight. The mean equivalent width, W, is given in equivalent angstroms; the mean measured central absorption, A_m, and the mean corrected central absorption, A_c, are given in percentages of the continuum. The average percentage deviation of any single measured W from the mean W for the line is ± 9.2 per cent of the mean W. The average deviation of any single central absorption from the mean measured central absorption for the line is ± 1.8 per cent of the continuum. The rather large average error in a single measurement of equivalent width reflects the graininess of the plates. It is advisable to use finer-grained plates than 103*a*-O if the brightness of the object and the speed of the spectrograph will permit. The average error in a measurement of central absorption is small and is of the order of the correction for instrumental profile. It is mostly caused by uncertainty in placing the continuum. Since the lines have relatively wide wings for their depths, this uncertainty in placing the continuum is sufficient to account for most of the uncertainty in the equivalent widths, as much of the equivalent width arises in the wings.

The equivalent widths of Table 2 may be compared with those of E. G. Williams.[6]

[6] *Ap. J.*, 83, 279, 1936.

We have 59 lines in common. The mean value of the ratio $(ABU - EGW)/ABU$ is -13.1 ± 2.9 per cent. Thus the present measures are a little smaller, on the average, than those of E. G. Williams. This is not surprising, as on microphotometer tracings of high-dispersion spectra one is inclined to draw the continuum low and thus cut off part of the extensive wings of the lines. This is particularly true when, as in the present case, only short regions of the plate around the lines of interest are run through the microphotometer. The comparisons given in the accompanying table are of interest. The mean value of the ratio $(ABU - x)/ABU$ with its probable error is tabulated, where x denotes the work to which comparison is being made. The equivalent widths of Table 2 are referred to as "*ABU*."

Lines	No. of Measures in Common	x	$(ABU-x)/ABU$
Hydrogen	10	E. G. Williams*	+ 1.1±5.2 per cent
Hydrogen	12	S. Günther†	− 6.5±5.3
He I	23	E. G. Williams*	−22.4±3.9
He I	10	A. B. Underhill‡	+ 9.2±4.4
Mg II, *Si* II, and *Si* III	26	E. G. Williams*	−10.2±6.6

* *Ap. J.*, **83**, 279, 1936.
† *Zs. f. Ap.*, **7**, 106, 1933. ‡ *J.R.A.S. Canada*, **38**, 385, 1944.

The rather large negative difference, −22.4 per cent, between the equivalent widths of the *He* I lines given in this paper and those given by E. G. Williams is partly due to his inability to resolve the blends at λ 4026 and λ 4144 on his dispersion. The effect of these blends is discussed in my earlier paper[7] on the *He* I lines. It would seem that the equivalent widths obtained from McDonald coudé plates are substantially in systematic agreement with measures of equivalent widths obtained elsewhere.

The equivalent widths given for λ 4471 in Table 2 for the main-sequence stars include the forbidden line λ 4470. On the profiles it is possible to estimate where the violet wing of λ 4471 might lie. If this is done, subtraction gives the equivalent width due to λ 4470. The equivalent widths obtained in this way are given in notes to Table 2. The mean measured central absorptions for λ 4470 are 24 in γ Peg, 17 in τ Her, and 11 in ζ Dra. The equivalent width of the whole feature at λ 4026 is given in Table 2 for the main-sequence stars. In γ Peg it is possible to separate on the profile the combined feature λ 4026 + the forbidden *He* I lines from λ 4024 of *He* I and the *Fe* III line at λ 4025. The equivalent width of λ 4026 + [*He* I] is given in a note to Table 2. In the supergiants λ 4024 and λ 4026 of *He* I can be seen clearly separated. There is a number of *O* II and *S* II lines in the wings of λ 4144. On coudé spectra one can resolve these features; hence the equivalent widths given in Table 2 for λ 4144 are for the *He* I line only, as the blending lines have been separated out.

The one plate for χ Aur, Cd684, is well exposed and should yield reliable equivalent widths and line profiles. In forming the mean values for η CMa, the plates Cd126 and Cd134 are not used, since on these plates some of the lines appear double and all the lines are shallower than usual. These plates were taken by Greenstein in February, 1941; and none of the plates taken at scattered intervals since that date have shown this phenomenon again. Although Cd126 and Cd134 are not very dense, it seems improbable that the observed line-shape changes are due to photographic effects. These two plates give a radial velocity near that obtained from the rest of the plates. At present there are insufficient data to discuss possible variations in the spectrum of η CMa further.

[7] *J.R.A.S. Canada*, **38**, 385, 1944.

The one plate for ζ Dra, Cd737, is of good density and should yield quite reliable measures.

i) *Hydrogen lines.*—The data in Table 2 show that the depths of the hydrogen lines in all the supergiants studied are around 50 per cent, whereas in the dwarf stars the central absorptions are deeper and increase from 62 per cent at B2.5 to about 80 per cent at B8. Typical profiles of $H\gamma$ for the supergiant stars are shown in Figure 1, and for the other stars in Figure 2. The difference in shape caused by Stark broadening in the stars of lower luminosity is obvious. Comparison of $H\gamma$ in ϵ CMa with $H\gamma$ in the supergiants shows that a luminosity class II star has hydrogen-line profiles quite different from those of the supergiants, the Stark wings already being prominent. The difference between luminosity classes I*a* and II is large. The stars ϵ CMa, γ Peg, and τ Her give profiles that are very much the same from plate to plate and, on the whole, symmetrical. However, the profiles of the hydrogen lines in the supergiants seem to change from plate to plate and tend to show small asymmetries which also change from time to time. For this reason a profile from one plate only is given for the supergiants, whereas a mean profile

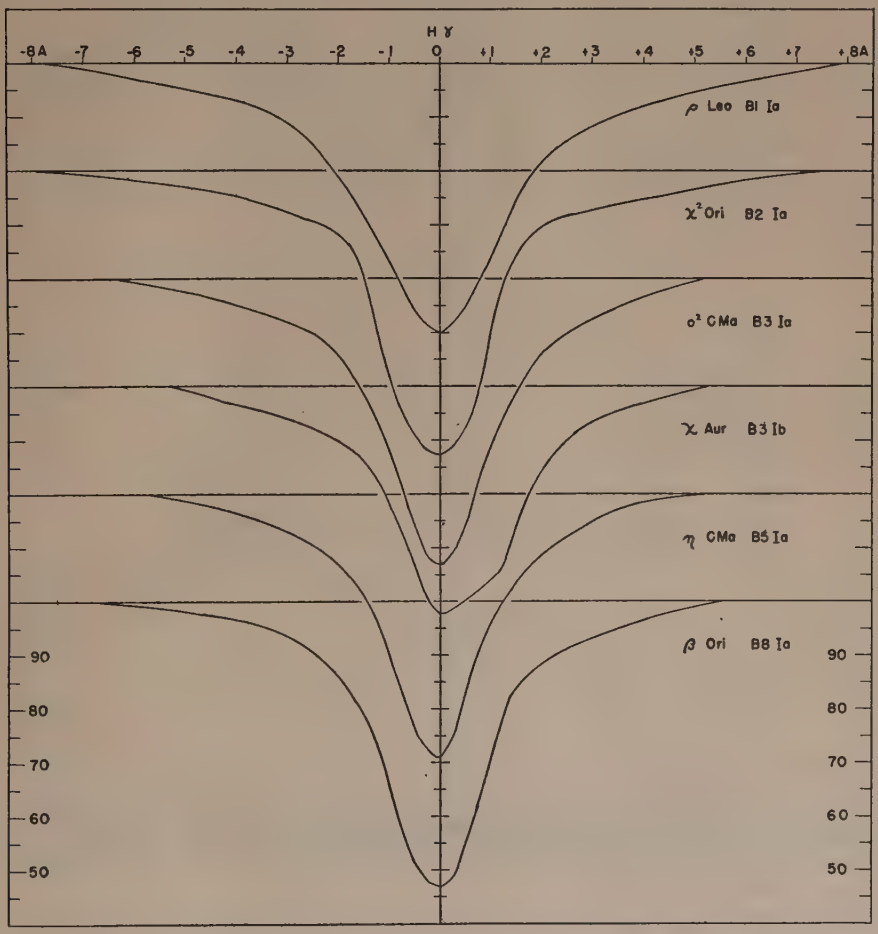

FIG. 1.—$H\gamma$ in the supergiants. The scale for residual intensity is given only for β Ori. Each profile is displaced 20 per cent below the preceding one. The residual intensity is in percentages of the continuum.

is drawn for the other stars. The slight variability and asymmetry of $H\gamma$ in χ^2 Ori and β Ori may be related to the fact that $H\alpha$ is in emission in these stars; and χ Aur has been reported to be a spectroscopic binary by R. K. Young,[8] which may account for the peculiar shape observed for $H\gamma$. There is no defect apparent on the plate or the microphotometer tracing that can account for the observed shape of the line. In χ Aur all the lines are weaker than in the comparable stars, o^2 CMa and ϵ CMa. It is possible that the observed weakening is due to the overlying spectrum of the companion.

ii) *Helium lines.*—The *He* I lines have been thoroughly discussed by many investigators.[9] The present observations are in accord with their results. The data of Table 2

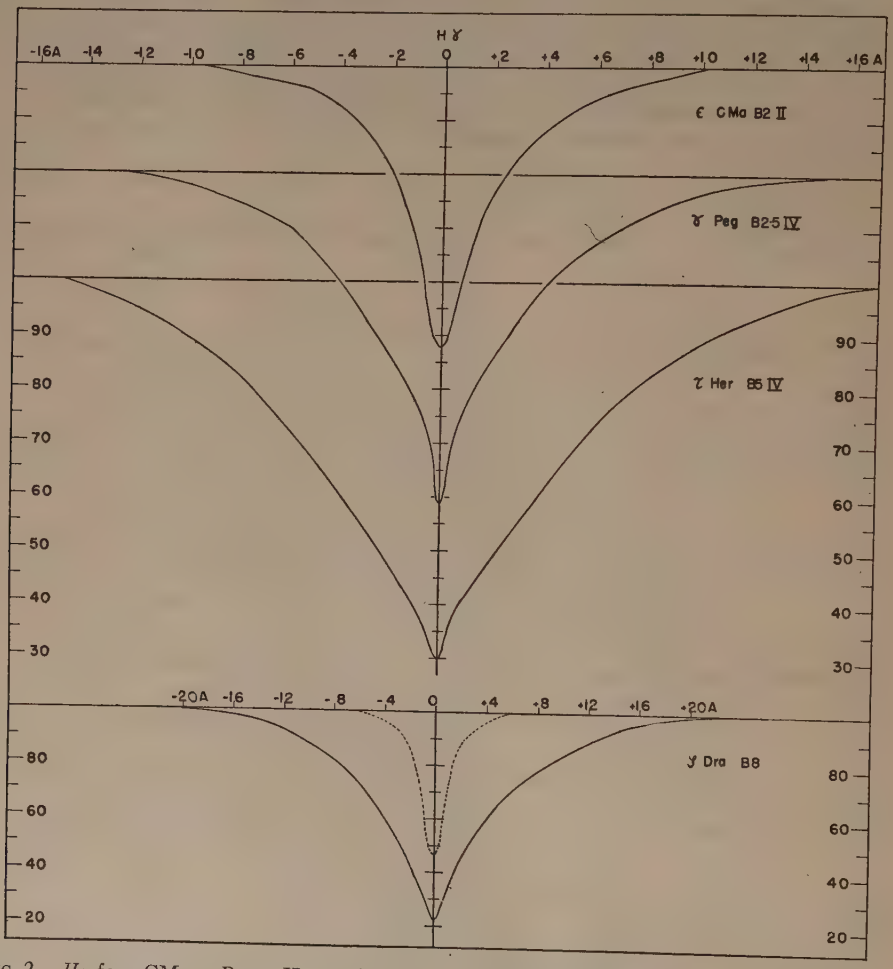

FIG. 2.—$H\gamma$ for ϵ CMa, γ Peg, τ Her, and ζ Dra. For ϵ CMa, γ Peg, and τ Her the wave-length scale is half its value in Fig. 1. For ζ Dra the wave-length scale has been reduced by a factor 4 from Fig. 1. The profiles for ϵ CMa, γ Peg, and τ Her are each displaced vertically by 20 per cent. The profile for β Ori, B8 Ia, is dotted in for comparison with $H\gamma$ in the main-sequence star ζ Dra. The residual intensity is in percentages of the continuum.

[8] *Pub. Dom. Obs., Ottawa*, **4**, 1, 1920.

[9] See, e.g., O. Struve, *Ap. J.*, **74**, 225, 1931; E. G. Williams, *Ap. J.*, **83**, 305, 1936; P. Rudnick, *Ap. J.*, **83**, 439, 1936; and A. B. Underhill, *J.R.A.S. Canada*, **38**, 385, 1945.

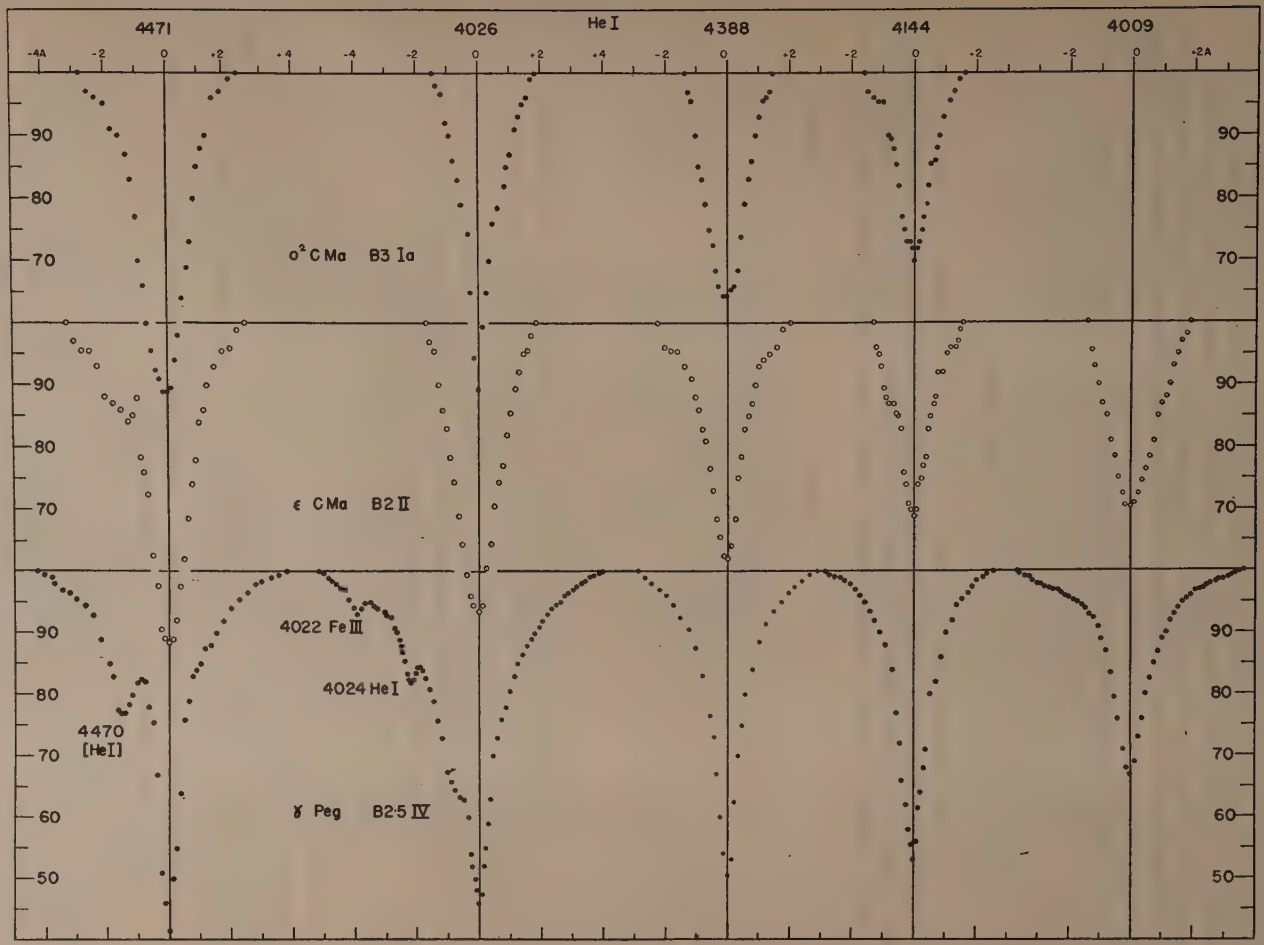

FIG. 3.—The *He* lines in o^2 CMa, ϵ CMa, γ Peg. The residual intensity is in percentages of the continuum

indicate the increase in equivalent width of the *He* I lines due to Stark effect as one goes from supergiants to main-sequence stars. The well-known maximum of the *He* I lines at about type B2 is better indicated in the main-sequence stars than in the supergiants. The observations indicate that at B2 the *He* I lines are deeper in the main-sequence stars than in the supergiants, whereas at B5 and B8 the *He* I lines are deepest in the supergiants. A decrease in central absorption with increasing serial number is indicated for the singlet lines. Since only two triplet lines are observed, a similar trend cannot be confirmed for the triplets. Figure 3 shows the profiles observed for the *He* I lines in o^2 CMa, ϵ CMa, and γ Peg. The development of the Stark wings as the luminosity of the star decreases is clearly indicated. The strong forbidden lines of *He* I are marked on the diagrams for γ Peg. The profiles for o^2 CMa are from Cd727, for ϵ CMa from Cd729, and for γ Peg from Cd461. This cross-section of line shapes at about type B2.5 is typical of the cross-sections at later types.

iii) *The Mg II line and the Si II and Si III lines.*—The data of Table 2 confirm and extend the observations of these lines made on lower-dispersion plates by other investigators.[9] At spectral types B2 and B5 the *Mg* II line λ 4481 is stronger in luminosity class I*a* than in class IV. At B8 there is little luminosity effect. The line strengthens generally

TABLE 3

RELATIVE INTENSITIES OF THE *Si* III LINES

Line	ρ Leo	χ^2 Ori	o^2 CMa	χ Aur	η CMa	ϵ CMa	γ Peg
λ 4552.....	1.92	2.26	1.70	2.12	2.00	1.64	1.84
λ 4568.....	1.49	1.71	1.49	1.81	1.58	1.36	1.27
λ 4574.....	1.00	1.00	1.00	1.00	1.00	1.00	1.00

toward class B8. At B2, λ 4481 is shallower in luminosity class I*a* than in class IV. At B5, λ 4481 is about the same depth in class I*a* and IV. At B8 it is deeper in class I*a* than it is in the main-sequence star.

The *Si* II lines λ 4128 and λ 4130 show a general strengthening from spectral type B2 to B8. The data of Table 2 indicate for all spectral types studied that the depths of the lines are about the same in supergiant and in main-sequence stars. The *Si* II and particularly the *Si* III lines vary sharply with spectral type; thus, in estimating differences of behavior due to luminosity differences, care must be taken to compare only stars of the same spectral type.

The *Si* III lines $\lambda\lambda$ 4552, 4568, and 4574 are first measurable at about B5 and increase in strength toward B1. They show a definite luminosity effect, being strongest in the supergiants. The depths of the lines increase from B5 to B1. At B2 the lines are deeper in class IV than in the other luminosity classes. Since the theoretical relative strengths of λ 4552, 4568, and 4574 are in the ratio 5:3:1, the observed relative intensities of these lines will indicate on what part of the curve of growth these lines fall. If the lines fall on the damping part, their relative intensities should be in the ratio $\sqrt{5}:\sqrt{3}:1$ or 2.24:1.73:1. Table 3 gives the relative intensities of the *Si* III lines; the intensity of λ 4574 is unity in each case. Only the values for χ^2 Ori are close to the ratios which would be expected if all the lines of the multiplet fell on the damping part of the curve of growth. However, the probable errors in the measures of equivalent width do not exclude observed relative intensities in the range 1.84–2.69 for λ 4552, and 1.42–1.84 for λ 4568 from being interpreted as pure damping gradients. It is probable that the lines lie on the transition part of the curve of growth. If the lines fell near the point where the curve of growth changes from the Doppler part to the transition part, one might expect the ratio λ 4568:λ 4574 to approach the value 3:1 for stars in which the *Si* III lines were weak.

Since there is no evidence of this behavior, it seems most likely that the *Si* III lines lie closer to the damping part of the curve of growth than to the Doppler part. From the evidence of Table 3 it is doubtful if damping is the predominant broadening agent for the *Si* III lines in any of the stars studied. This view is supported by the fact that the line profiles do not show damping wings.

The relative intensities of the lines in the *Si* III multiplet have been investigated by I. H. Abdel-Rahman.[10] If his relative intensities are expressed in the same form as are the relative intensities in Table 3, they are seen to be closely the same as the data given here. He finds that an abnormally large damping constant is required if the lines are to lie on the damping portion of the curve of growth. It is more probable that λ 4574 does not lie on the damping part of the curve of growth; then such a large damping constant is not required to account for the observations. The present data and the more extensive data of Abdel-Rahman agree in indicating that λ 4574, and possibly λ 4568 in some cases, are relatively too strong for the multiplet to lie completely on the damping part of the curve of growth.

Typical line profiles for λ 4481 and the *Si* lines at about spectral type B2.5 are shown in Figure 4. The profiles are from the same plates that were used to give the *He* I line contours. The change of shape in going from luminosity class I*a*, o^2 CMa, to class II, ϵ CMa, to class IV, γ Peg, is conspicuous. However, its direct interpretation is difficult. Observed points are plotted in Figures 3 and 4.

In Table 4 are given the half half-widths of the *Mg* and *Si* lines, calculated according to equation (5) from the data of Table 2. These could be interpreted literally as Doppler widths if we knew the relation between the true profiles and the absorption coefficient. Expressed as velocities, these half half-widths, particularly for the supergiants, are quite large. In any case, these numbers, being proportional to W/A_c, give a measure of the sharpness of the lines. It is interesting to note that, although the *Mg* II line λ 4481 is a close doublet, it is very little wider on the average than the *Si* lines are. However, it is notable that the lines in the supergiants are generally wider than those in the less luminous stars. The numbers given for γ Peg indicate a minimum sharpness, as the central absorptions in this case have not been corrected for the instrumental profile. The broad lines in ρ Leo are largely due to rotation,[2] but the source of broadening for the other supergiants is difficult to decide. The effects of turbulence,[11] of expansion or contraction of the atmosphere,[12] and of the sphericity of the atmosphere[13] should all be considered. First, it should be demonstrated whether the ordinary theory of radiation transfer and line formation predicts suitable contours for the lines in B stars when adequate account is taken of collision and radiation damping, as well as of pure Doppler broadening. If it does not, then the above phenomena must be invoked to account for the observed line shapes.

3. *The interpretation of the line profiles.*—It can be shown[14] that, if Stark broadening is important, the line-absorption coefficient per atom in state $n = 2$ for the wings of the Balmer lines of hydrogen may be represented by

$$k^{(S)}(\Delta\lambda) = C\,\frac{F_0^{3/2}}{(\Delta\lambda)^{5/2}}, \tag{6}$$

where F_0 is the "normal field strength" and depends on the density of charged particles and their velocity and $\Delta\lambda$ in angstroms is the distance from the center of the line. The

[10] *M.N.*, **101**, 312, 1941.

[11] Struve and Elvey, *Ap. J.*, **79**, 409, 1934.

[12] Underhill, *Ap. J.*, **106**, 128, 1947. [13] *Ibid.*, **107**, 247, 1948.

[14] See Unsöld, *Physik der Sternatmosphären* (Berlin: Julius Springer, 1938), pp. 180 ff.

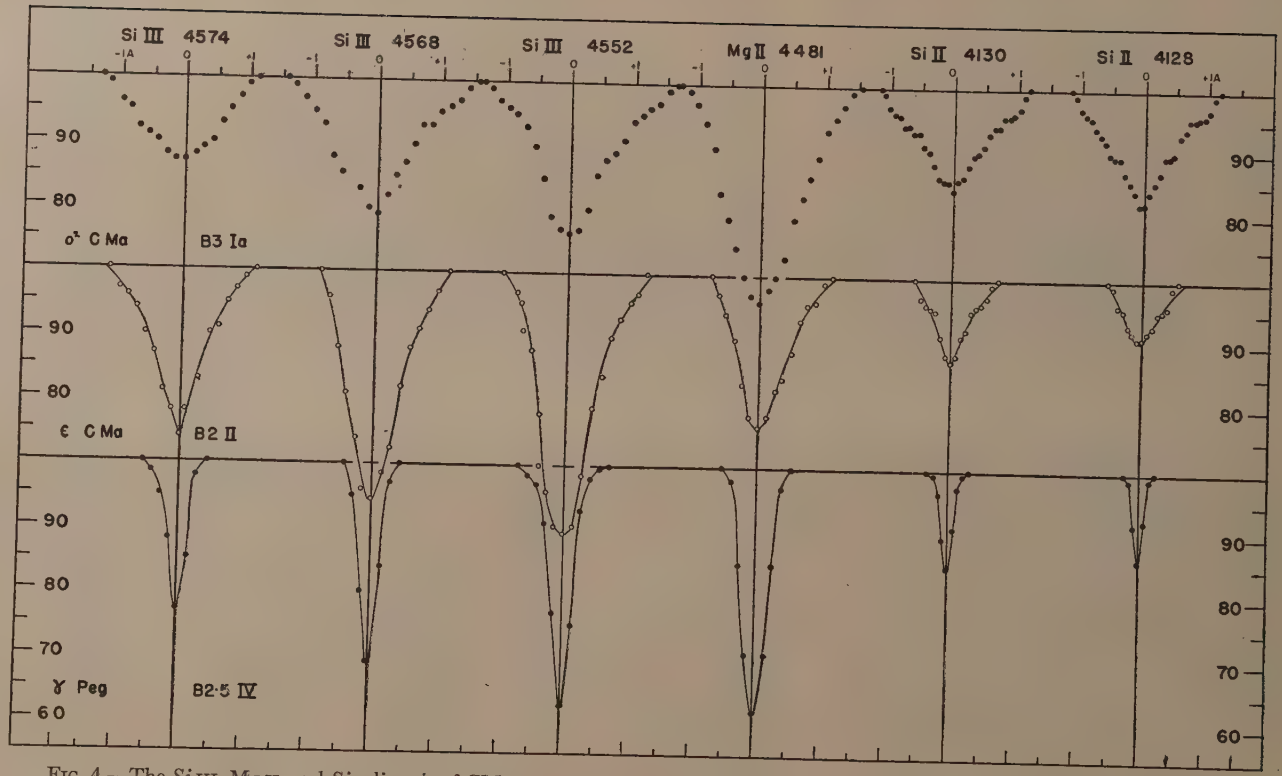

FIG. 4.—The *Si* III, *Mg* II, and *Si* II lines in o^2 CMa, ϵ CMa, and γ Peg. The residual intensity is in percentages of the continuum

constant C is evaluated by Unsöld for several of the Balmer lines. Inserting the numerical values given by Unsöld, we find for $H\gamma$ that

$$k^{(S)}(\Delta\lambda) = 1.42 \times 10^{-14} \frac{p_e}{T} (\Delta\lambda)^{-5/2}, \quad (7)$$

where p_e is the electron pressure in bars and T is the temperature. This expression differs from that quoted by Unsöld by a factor 2, since now it is known that only the field from protons causes the broadening of the hydrogen lines. The electrons do not contribute to the Stark effect of the hydrogen lines in the high-temperature stars.

Following Unsöld's discussion of radiation damping,[15] we see that, if radiation damping is important in forming the wings of the Balmer lines of hydrogen, the line-absorption coefficient per atom in state $n = 2$ for the wings of $H\gamma$ is

TABLE 4

HALF HALF-WIDTHS OF THE *Mg* AND *Si* LINES IN ANGSTROMS

Star	*Mg* II λ 4481	*Si* II λ 4130	*Si* II λ 4128	*Si* III λ 4574	*Si* III λ 4568	*Si* III λ 4552
ρ Leo	0.98A	.....	.....	0.82A	0.89A	0.96A
χ^2 Ori	.74	.....	.....	.67	.80	.89
σ^2 CMa	.73	0.71A	0.63A	.78	.78	.76
χ Aur	.80	.55	.59	.44	.56	.57
η CMa	.74	.58	.53	.57	.60	.60
β Ori	.63	.52	.53	.....	.....	.....
ε CMa	.49	.31	.33	.55	.53	.56
γ Peg	.26	.09	.08	0.22	0.20	0.25
τ Her	.55	.51	.48	.....	.....	.....
ζ Dra	0.64	0.60	0.52	.....	.....	.....

$$k^{(R)}(\Delta\lambda) = 7.31 \times 10^{-18} (\Delta\lambda)^{-2}, \quad (8)$$

where the appropriate numerical values for $H\gamma$ have been introduced. For radiation damping to be predominant we must have

$$k^{(R)}(\Delta\lambda) \geqslant k^{(S)}(\Delta\lambda). \quad (9)$$

This leads to the inequality

$$\frac{p_e}{T} \leqslant 5.12 \times 10^{-4} (\Delta\lambda)^{1/2}. \quad (10)$$

The maximum values that log p_e may reach if at $\Delta\lambda = 1$ A, or at $\Delta\lambda = 4$ A, the line-absorption coefficient is to be determined chiefly by radiation damping are given in Table 5. Since the expected electron pressures in B-type stars are greater than these values, it follows that the hydrogen-line profiles even in supergiants should be predominantly determined by Stark effect. Acting upon this assumption, Unsöld[16] derived electron pressures for a number of B-type stars. He derived[17] a relation between the equivalent width of a hydrogen line and the electron pressure, by using the empirical formula

$$\frac{1}{A} = \frac{1}{A_c} + \frac{1}{x_\nu}, \quad (11)$$

[15] *Ibid.*, pp. 152 ff. [16] *Zs. f. Ap.*, **23**, 100, 1944. [17] *Ibid.* **21**, 22, eqs. (27)-(31). 1944.

where A is the absorption at any point in the line, A_c is the central absorption, and

$$x_\nu = k^{(S)}(\Delta\lambda) N_{0,2} H , \tag{12}$$

is the optical thickness of the equivalent Schuster atmosphere. Here $N_{0,2}H$ is the number of hydrogen atoms in the second quantum state. Since we have profiles of the hydrogen lines, we may test the validity of Unsöld's assumptions. From equations (6) and (12) we note that, when Stark broadening is important,

$$\frac{1}{x_\nu} = \text{Constant}\,(\Delta\lambda)^{5/2}; \tag{13}$$

hence a plot of log $1/x_\nu$ as obtained from equation (11) against log $\Delta\lambda$ should yield a straight line with slope 5/2. If radiation damping is the most important broadening agent, we should get a straight line with slope 2.

TABLE 5

MAXIMUM ELECTRON PRESSURES IF RADIATION DAMPING IS TO PREDOMINATE

T	(log p_e)$_{max}$		T	(log p_e)$_{max}$	
	$\Delta\lambda = 1$ A	$\Delta\lambda = 4$ A		$\Delta\lambda = 1$ A	$\Delta\lambda = 4$ A
10,000°	0.71	1.01	20,000°	1.01	1.31
16,000°	0.92	1.21	24,000°	1.09	1.39

Figure 5 shows such plots for $H\gamma$ in o^2 CMa, ϵ CMa, and γ Peg. The points are chosen for $\Delta\lambda \gtrsim 1$ A. The slope of the best straight line for o^2 CMa is 2.05, for ϵ CMa it is 1.53, and for γ Peg it is 1.91. In the latter case one has no doubt that the profile is the result of Stark effect. The two or three points in each case to the right of log $[(1/A) - (1/A_c)] = 1.2$ represent absorptions of less than 5 per cent; hence it is not significant that they deviate from the straight line. Similar results are obtained from the profiles of $H\gamma$ and $H\delta$ in the other stars. The slope is generally less than 2 and is in no case greater than 2.3. Since we expect that even in the supergiants the absorption coefficient is largely determined by Stark effect, we must conclude that equation (11) does not represent the process of line formation for the hydrogen lines in B stars. Consequently, electron pressures deduced from formulae based on equation (11) should be regarded only as indications of order of magnitude.

We shall now investigate an atmosphere in which the classical temperature distribution of a gray body is valid, and we shall show how the intensities of some typical lines may be computed. Chandrasekhar[18] has shown that the gray-body temperature distribution remains valid in a nongray atmosphere to a good approximation if the proper mean absorption coefficient,

$$\bar{\kappa} = \int_0^\infty \kappa_\nu \frac{F_\nu^{(1)}}{F}\, d\nu , \tag{14}$$

is used. In forming $\bar{\kappa}$, the monochromatic absorption coefficients are weighted by the monochromatic fluxes in a gray body. It has been assumed that

$$\frac{\kappa_\nu}{\bar{\kappa}} = \delta_\nu + 1 , \tag{15}$$

[18] *Ap. J.*, **101**, 328, 1945.

where δ_ν, a small quantity independent of depth, measures the departure from grayness. The relation (14) has been developed for an atmosphere in which the equation of transfer,

$$\cos\vartheta \frac{dI_\nu}{\rho dz} = -\kappa_\nu I_\nu + \kappa_\nu B_\nu , \tag{16}$$

is valid. For a B-type atmosphere, electron scattering is important; hence the appropriate equation of transfer is

$$\cos\vartheta \frac{dI_\nu}{\rho dz} = -(\kappa_\nu + \sigma) I_\nu + \kappa_\nu B_\nu + \sigma J_\nu , \tag{17}$$

where σ is the electron-scattering coefficient and is independent of frequency. It can be shown, following Chandrasekhar,[18] that the gray-body temperature distribution can be

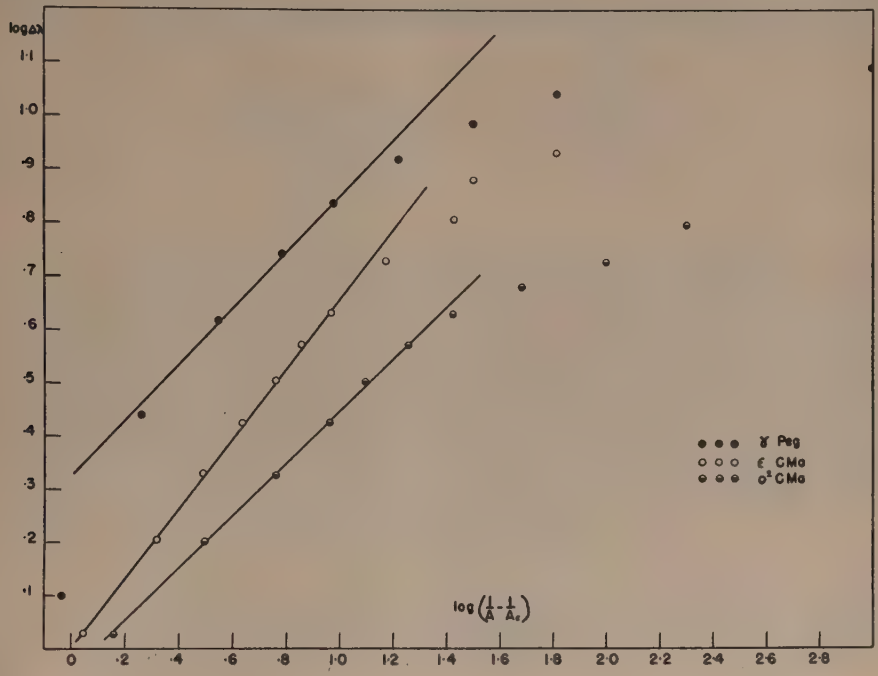

FIG. 5.—Log $\left(\frac{1}{A}-\frac{1}{A_c}\right)$ − log Δλ plots for $H\gamma$ in o^2 CMa, ϵ CMa, and γ Peg. Δλ is measured in angstroms.

maintained as a good approximation if the optical depth, τ, is given by

$$d\tau = -(\bar{\kappa} + \sigma)\, \rho dz , \tag{18}$$

where $\bar{\kappa}$ is the mean absorption coefficient defined in equation (14) and there are the same restrictions on δ_ν, the departure from grayness, as before.

We shall consider a pure hydrogen atmosphere with boundary temperature $\theta_0 = 0.30$. The monochromatic mass absorption coefficient per gram of star material is

$$\kappa_\nu = k_\nu (1 - x) , \tag{19}$$

where k is the mass absorption coefficient per gram of neutral hydrogen (corrected for stimulated emissions), and $1-x$ is the fraction of neutral hydrogen atoms at any level in the star. The quantity $1-x$ is obtained from the ionization equation for hydrogen and is dependent on the temperature and electron pressure. The absorption coefficient k is dependent only on the temperature. The electron-scattering coefficient per gram of star material, σ, is given by

$$\sigma = \sigma_e \frac{x}{m_H}, \tag{20}$$

where σ_e is the electron-scattering coefficient per electron. For the temperatures and pressures of the atmospheres to be investigated, hydrogen is so highly ionized that

$$\sigma = \text{Constant} = 0.40 \tag{21}$$

throughout.

We evaluate the mean absorption coefficient by putting

$$\bar{\kappa} = \bar{k}\,(1-x) = (1-x)\frac{\int_0^{\nu_1} k_\nu \frac{F_\nu^{(1)}}{F}\,d\nu}{\int_0^{\nu_1} \frac{F_\nu^{(1)}}{F}\,d\nu}, \tag{22}$$

where ν_1 is the frequency of the Lyman limit. If the integration is carried out over all frequencies less than the Lyman limit, the departures from grayness are always small. If the integration is performed over frequencies from zero to infinity as in equation (14), then, because k is very large in the Lyman continuum and $F_\nu^{(1)}$ is not vanishingly small, the part of the integral with ν running from ν_1 to infinity will far outweigh the rest of the integral, and the departures from grayness in the usual regions will become large. Since the fraction of the total flux emergent in the Lyman continuum is not very large, it is permissible to neglect this flux in an approximate theory. In this way $\bar{k}$ was calculated at $\tau = 0$, 0.5, and 1.0. The classical relation

$$T^4 = T_0^4\,(1+\tfrac{3}{2}\tau) \tag{23}$$

was assumed.

Since hydrogen is almost completely ionized, we can write

$$p_e = \tfrac{1}{2}p\,, \tag{24}$$

where p is the total pressure. If radiation pressure is neglected, the equation of hydrostatic equilibrium gives

$$\frac{dp_e}{d\tau} = \frac{g}{2}\frac{1}{\bar{\kappa}+\sigma}, \tag{25}$$

where g is the surface gravity. We have

$$\bar{\kappa} = \bar{k}\,(\tau)\,(1-x)\,, \tag{26}$$

where $\bar{k}(\tau)$ is known graphically as a function of τ from the calculations discussed above and $1-x$ is a known analytic function of τ and p_e. To obtain p_e as a function of optical depth, an initial p_e, compatible with the surface gravity and mean absorption coefficient, is assumed, and equation (25) is integrated step by step. Each stage is iterated to get

the best dp_e before advancing to the next stage of the integration. When p_e has been determined, $\bar{\kappa}+\sigma$ and $\kappa_\nu+\sigma$ are obtained at each optical depth, and thence the ratio

$$n_\nu = \frac{\kappa_\nu + \sigma}{\bar{\kappa} + \sigma} \tag{27}$$

is found. If the standard theory of line formation is to be used, strictly this ratio should be independent of optical depth. However, small variations of n_ν will not invalidate the theory. In order to predict the intensity at any point in a line, the ratio

$$\eta_\nu = \frac{l_\nu}{\kappa_\nu + \sigma}, \tag{28}$$

where l_ν is the line-absorption coefficient per gram of star material, must be known. Strömgren[19] has shown that, if η_ν is reasonably constant with increasing optical depth, the residual intensity at any point in the line is given by

$$R_\nu = \frac{1 + \frac{2}{3}\sqrt{3}}{\frac{4}{3}\sqrt{3} + \frac{1}{2}\frac{x_0}{n_\nu}} \frac{\frac{4}{3}\sqrt{3}\,\overline{\sqrt{\lambda_\nu}} + \frac{1}{2}\frac{x_0}{n_\nu}\overline{\lambda_\nu}}{1 + \frac{2}{3}\sqrt{3}\,\overline{\sqrt{\lambda_\nu}}}, \tag{29}$$

where

$$x_0 = \frac{h\nu}{kT_0}(1 - e^{-h\nu/kT_0})^{-1}, \tag{30}$$

and

$$\lambda_\nu = \frac{1}{1 + \eta_\nu}. \tag{31}$$

The quantities $\bar{\lambda}_\nu$ and $\overline{\sqrt{\lambda}_\nu}$ are suitable mean values of λ_ν and $\sqrt{\lambda_\nu}$. In a later paper[20] Strömgren gives a practical method of forming these mean values by using the weighted values of λ_ν and $\sqrt{\lambda_\nu}$ at five representative points. Equation (29) has been derived on the assumption that absorption plays no role in line formation but that the lines are formed by a pure scattering process. That is, the quantity ϵ, which is usually introduced to allow for the absorption processes, has been put equal to zero.

The line-absorption coefficient in the center of a line is given by

$$l_{\text{center}} = \frac{\sqrt{\pi}\,e^2}{mc}\frac{f}{v}\lambda\frac{N^*}{N}N, \tag{32}$$

where

$$v = 1.289 \times 10^4 \sqrt{\frac{T}{\mu}}\ \text{cm/sec} \tag{33}$$

is the most probable thermal velocity of the atoms, N^*/N is the relative number of atoms excited to the lower level of the line, and N is the number of atoms per gram of star material in the proper stage of ionization. (Here λ is the wave length of the line.) The quantity μ is the atomic weight of the atom in question. Table 6 gives θ, log p_e, log $(1-x)$, $\bar{\kappa}+\sigma$, and n_ν at λ 4340 as functions of τ for an atmosphere in which log $g = 4.09$; also given are log η at the center of the *Si* II line λ 4128, the *Si* III line λ 4552,

[19] *Ap. J.*, 86, 1, 1937.

[20] *Pub. Copenhagen Obs.*, No. 127, p. 243, 1940.

the *He* I line λ 4471, and $H\gamma$. The *f*-values of the silicon lines and the relative abundance by number, $a(Si)$, of silicon are unknown. The tabulated η's are for the case in which $fa(Si) = 10^{-6}$. Similarly, the relative abundance by number, $a(He)$, of helium must be known; it is assumed to be 10^{-1}, and the *f*-value for λ 4471 given by Goldberg[21] is used. A model in which log $g = 2.00$ is given in Table 7.

TABLE 6

$\theta_0 = 0.300$; LOG $g = 4.09$

τ	θ	LOG p_e	LOG $(1-x)$	$\bar{\kappa}+\sigma$	n_ν λ 4340	LOG η_{center}				WING OF $H\gamma$ LOG η(4 A)
						Si II* λ 4128	*Si* III* λ 4552	*He* I† λ 4471	*H* λ 4340	
0.01...	0.299	1.70	−4.34	1.21	0.717	+0.34	0.85	2.84	3.29	−0.82
0.02...	.298	1.94	−4.13	1.72	0.686	+0.47	.74	2.99	3.37	−0.51
0.04...	.296	2.15	−3.95	2.46	0.650	+0.56	.62	2.96	3.41	−0.26
0.06...	.294	2.26	−3.87	3.02	0.871	+0.34	.55	2.83	3.39	−0.17
0.08...	.292	2.34	−3.83	3.45	0.863	+0.39	.52	2.85	3.38	−0.10
0.10...	.290	2.40	−3.80	3.81	0.811	+0.42	.48	2.87	3.38	−0.04
0.20...	.281	2.59	−3.77	4.66	0.989	+0.32	.38	2.81	3.33	+0.09
0.40...	.267	2.80	−3.80	5.07	1.21	+0.28	.52	2.81	3.26	+0.22
0.60...	.256	2.94	−3.86	4.96	1.46	+0.21	.61	2.79	3.15	+0.32
0.80...	.246	3.06	−3.91	4.68	1.81	+0.09	.67	2.76	3.20	+0.40
1.00...	0.238	3.15	−3.96	4.48	2.06	−0.08	0.92	2.75	3.21	+0.50

* $fa(Si) = 10^{-6}$.
† $a(He) = 10^{-1}$.

TABLE 7

$\theta_0 = 0.300$; LOG $g = 2.00$

τ	θ	LOG p_e	LOG $(1-x)$	$\bar{\kappa}+\sigma$	n_ν λ 4340	LOG η_{center}				WING OF $H\gamma$ LOG η(4 A)
						Si II* λ 4128	*Si* III* λ 4552	*He* I† λ 4471	*H* λ 4340	
0.01.....	0.299	0.08	−5.97	0.419	0.981	−1.66	0.55	1.60	1.60	−3.75
0.02.....	.298	0.37	−5.69	.436	0.966	−1.15	0.75	1.87	1.88	−3.19
0.04.....	.296	0.66	−5.44	.466	0.966	−0.71	0.90	2.11	2.13	−2.69
0.06.....	.294	0.82	−5.31	.494	0.972	−0.82	0.92	2.21	2.36	−2.32
0.08.....	.292	0.93	−5.24	.518	0.960	−0.65	0.97	2.30	2.43	−2.15
0.10.....	.290	1.02	−5.18	.539	0.946	−0.53	1.00	2.34	2.49	−2.03
0.20.....	.281	1.27	−5.08	.605	0.996	−0.51	0.94	2.46	2.68	−1.65
0.40.....	.267	1.54	−5.07	.651	1.09	−0.49	1.08	2.54	2.78	−1.40
0.60.....	.256	1.70	−5.11	.657	1.20	−0.63	1.07	2.56	2.84	−1.21
0.80.....	.246	1.82	−5.14	.652	1.32	−0.86	1.00	2.55	2.96	−1.08
1.00.....	0.238	1.92	−5.19	0.639	1.43	−1.17	1.11	2.53	2.94	−0.97

* $fa(Si) = 10^{-6}$.
† $a(He) = 10^{-1}$.

[21] *Ap. J.*, 90, 414, 1939.

In the wing of $H\gamma$ the line-absorption coefficient per gram of star material is

$$l(\Delta\lambda) = 1.42 \times 10^{-14} \frac{p_e}{T} (\Delta\lambda)^{-5/2} \frac{N_H(2)}{N} \frac{(1-x)}{m_H} \tag{34}$$

(cf. eq. [7]), where $N_H(2)/N$ is the relative number of hydrogen atoms in the state $n = 2$, and m_H is the mass of a hydrogen atom. Here $\Delta\lambda$ is in angstroms. From this expression $\eta(\Delta\lambda)$ may be obtained. Log η(4 A) for the two models is given in the last columns of Tables 6 and 7.

In the log $g = 4.09$ model, η for *Si* II increases inward at first for a short distance and then decreases regularly as greater optical depths and higher ionization are reached. For *Si* III the trend of η with τ is the opposite of this, η decreasing rapidly at first as the increasing electron pressure decreases the ionization, and then increasing again as the effects of increasing temperature predominate. For *He* I and the center of $H\gamma$, η is reasonably constant with increasing optical depth. In these two cases η is so large that complete absorption effectively occurs at the outermost fringes of the atmosphere. In the wing of $H\gamma$, the line-absorption coefficient is pressure-dependent; thus η increases rapidly with increasing optical depth. Since $\eta(\Delta\lambda)$ can be obtained from η(4 A) by multiplying η(4 A) by $4^{5/2}(\Delta\lambda)^{-5/2}$, η has quite different values at different points in the wing of the line.

In the log $g = 2.00$ model, the variations of η with increasing depth are greater in all cases than in the log $g = 4.09$ model. The *Si* II line is weakened with respect to the *Si* III line because of the low electron pressure which favors the ionization of *Si* II. For *Si* II, η reaches a maximum at a greater depth than in the log $g = 4.09$ model. For *Si* III, η rises rapidly with increasing optical depth and at a τ of about 0.08 becomes nearly independent of optical depth. The η for *He* I, λ 4471, behaves in a similar manner. It is smaller than in the log $g = 4.09$ model, because at the low pressures of the log $g = 2.00$ model the ionization of helium is advanced. The η_{center} for H behaves similarly and shows the advancement of the ionization of hydrogen in the log $g = 2.00$ model. Thus, apart from the broadening effects of Stark effect which must be considered in the denser model, we should expect the helium and hydrogen lines to be weaker in early supergiants than in main-sequence stars of the same temperature, because there are fewer neutral atoms to absorb the lines. Observations[7] of λ 5876, the leading member of the triplet diffuse series of *He* I, do not confirm this conclusion for helium, the line being significantly stronger in the early supergiants than in the main-sequence stars. Since this line is very little affected by Stark effect, we should expect abundance effects, such as those indicated above, to be detectable. To account for the observations, we might postulate some strong broadening agent in the supergiant stars or that there is some process, such as proposed by Foster and Douglas,[22] making λ 5876 abnormally weak in the main-sequence stars. We should also recognize that λ 5876 may have a tendency to appear in emission in some supergiants, much as $H\alpha$ does. In the wing of $H\gamma$, in the log $g = 2.00$ model, η varies very greatly with increasing optical depth. We have considered Stark broadening only as a broadening agent. At the low pressures of this model it is possible that some other source of broadening may be dominant. A comparison of the predicted profile with observations may indicate whether this is so.

Equation (29) has been used to predict absorptions for the various lines from the values of η tabulated in Tables 6 and 7. The predicted absorptions are given in Table 8. They are listed as A_5 when $\bar{\lambda}_\nu$ and $\overline{\sqrt{\lambda_\nu}}$ have been found from the values of λ_ν and $\sqrt{\lambda_\nu}$ at five representative points as suggested by Strömgren, and as A_1 when the values of λ_ν and $\sqrt{\lambda_\nu}$ at one optical depth have been inserted in equation (29). In this latter case

[22] *M.N.*, 99, 150, 1939.

the atmosphere is assumed to be homogeneous, with the properties of the model atmosphere at the one representative point. The single representative point in the log $g = 4.09$ model is at $\tau = 0.11$. For the log $g = 2.00$ model, the single representative point is at $\tau = 0.22$. The selection of these single representative points is arbitrary, and the intention of their use is to show the effects of stratification. When η changes fairly rapidly with optical depth, the predicted absorptions are sensitive to the representative points chosen. The difference of A_1 from A_5 illustrates this point.

Log g for a star can be estimated from the prediction of the wings of $H\gamma$ and from the relative intensities of the silicon lines. Thus comparison of the observed profile for $H\gamma$ in γ Peg with the predicted absorptions, A_5, in both models, suggests a value of g intermediate between the two values chosen. The predicted relative central absorptions of the silicon lines also suggest this. When the mean of the observations for χ^2 Ori and o^2 CMa are compared with the predicted $H\gamma$ in the log $g = 2.00$ model, it would seem that log $g = 2.00$ is a fairly good estimate for the supergiants. If the predicted points are plotted to form a profile, the shape of the predicted line is rather different from the observed shape, and there is a question of whether there is some other broadening agent active.

TABLE 8

PREDICTED ABSORPTIONS

Line	log $g = 4.09$		log $g = 2.00$		Wing of $H\gamma$ $\Delta\lambda$	log $g = 4.09$			log $g = 2.00$		
	A_{c_5}	A_{c_1}	A_{c_5}	A_{c_1}		A_5	A_1	A_{obs}	A_5	A_1	A_{obs}
Si II λ 4128...	36	42	7	10	1 A.....	69	78	42	20	20	32
Si III λ 4552..	43	43	58	63	2.....	50	55	34	8	4	13
He I λ 4471...	95	95	83	92	4.....	26	24	21	3	2	4
H λ 4340.....	97	97	87	95	8.....	2	8	7	.....	.....	.....

The absorption coefficient from radiation damping only is comparable in size to that from Stark broadening for the low electron pressures of the log $g = 2.00$ model. The observed relative central absorptions of the *Si* II lines suggest a slightly larger g-value than that used in the model. However, since the observations show that the shape of $H\gamma$ in supergiants is significantly different from the shape of $H\gamma$ in main-sequence stars, g cannot be increased much, or the typical Stark-broadened shape will result.

When a reasonable estimate of log g has been made in this way, abundances of the elements may be derived by finding that abundance which will give a predicted profile which fits the observed profile. Such a procedure would not entail a prohibitive amount of work, for the abundance enters η as a multiplicative factor only. This method of finding abundances has the advantage that account may be taken of the variation of η through the atmosphere, that is, of stratification, if it is important, and use is made of the shape of the absorption line, as well as of its equivalent width. We are assuming that the boundary temperature θ_0 is known. In practice the best pair of θ_0 and log g can be estimated by fitting the wings of the hydrogen lines; and then the relative abundances of the elements can be derived upon the assumption of a suitable form for the line-absorption coefficient. If the f-value of the line is not known, then it is the product of the f-value and the abundance that will be determined. This method of determining abundances should be quite critical for elements which are present in two stages of ionization, for then the intensities of the lines in both spectra must be predicted satisfactorily.

Our model atmosphere computations also allow us to derive the shape of the line-absorption coefficient from observations. When the predicted values of A_1 are plotted

against η and the predicted A_5 are plotted against $\bar{\eta}$, where $\bar{\eta}$ is the value of η corresponding to $\bar{\lambda}_\nu$, both sets of points are found to lie on a single curve with very little scatter. The same curve can be used for both models up to absorptions of about 60 per cent. The reason that one curve can be so constructed is that the predicted absorptions are not very sensitive to the change of darkening, $\frac{1}{2}x_0/n_\nu$, with wave length or gravity, or to a fairly large variation of η with optical depth. The values of η corresponding to the observed absorptions in a line profile can be read from this mean curve, as a function of $\Delta\lambda$, the displacement from the center of the line. The variation of η with $\Delta\lambda$ will represent the variation of the line-absorption coefficient with $\Delta\lambda$. Since we have seen that

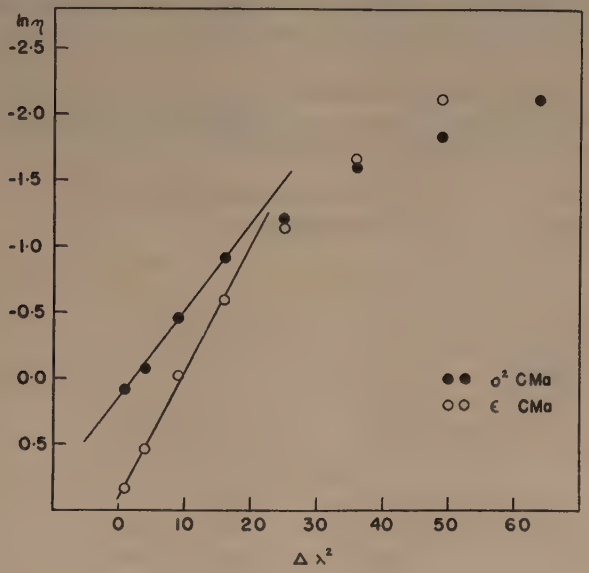

FIG. 6.—$ln\,\eta - (\Delta\lambda)^2$ plot for λ 4552 in o^2 CMa and ε CMa. Δλ is expressed as millimeters on the microphotometer tracing.

the line profiles have very closely a Gaussian shape, we shall see if $\eta(\Delta\lambda)$ itself is Gaussian. Let us assume

$$\eta = \eta_0\, e^{-(\Delta\lambda/\Delta\lambda_D)^2}\,, \tag{35}$$

where λ_D is the width of the line-absorption coefficient due to the most probable velocity of the atoms. Then

$$ln\,\eta = ln\,\eta_0 - \left(\frac{\Delta\lambda}{\Delta\lambda_D}\right)^2; \tag{36}$$

hence a plot of $ln\eta$ against $(\Delta\lambda)^2$ should yield a straight line with slope $(\Delta\lambda_D)^{-2}$, if the line-absorption coefficient is Gaussian in shape. The intercept at $\Delta\lambda = 0$ gives η_0, from which the abundance of the element may be deduced if the f-value of the line is known. Figure 6 gives such plots for λ 4552 in o^2 CMa and ε CMa. The core of the line can be represented by a Gaussian line-absorption coefficient, but in the wings the form of the line-absorption coefficient may be different. The present observations are not accurate enough to determine unambiguously the shape of the absorption coefficient in the wings of the lines, as in the wings the uncertainty in any measure of absorption is a large

fraction of the measured absorption. Such plots were made for the *Si* II and *Si* III lines in o^2 CMa and ϵ CMa; and $\Delta\lambda_D$ in kilometers per second was derived from the slope of the first part of the curve. The mean $\Delta\lambda_D$ from the five determinations in each case is 37 ± 2 km/sec for o^2 CMa, and 27 ± 2 km/sec for ϵ CMa. These values, if interpreted as turbulent velocities, are considerably larger than the mean values of v_t found by Goldberg[23] from curves of growth for B2 supergiants. They are significantly less than the half half-widths of Table 4 give, if these half-widths are interpreted directly as $\Delta\lambda_D$. This is because the relation between absorption and line-absorption coefficient is not, in general, linear. The large Doppler widths of the lines in the supergiant o^2 CMa and the giant ϵ CMa appear to be an example of the phenomenon discussed by Struve,[24] K. O. Wright,[25] and M. Schwarzschild[26] for F supergiants—that the lines are broader than the turbulent velocity found from the curve of growth would suggest.

I am very grateful to Dr. Jesse L. Greenstein for many helpful and fruitful discussions of the problems dealt with here. His encouragement and aid in dealing with the problems of line interpretation are particularly acknowledged.

[23] *Ap. J.*, **89**, 623, 1939.

[24] *Ap. J.*, **104**, 138, 1946.

[25] *J.R.A.S. Canada*, **41**, 49, 1947

[26] Unpublished.

Reprinted for private circulation from
THE ASTROPHYSICAL JOURNAL
Vol. 107, No. 2, March 1948
PRINTED IN THE U.S.A.

THE SCHUSTER PROBLEM FOR AN EXTENDED ATMOSPHERE

ANNE B. UNDERHILL*
Yerkes Observatory
Received December 26, 1947

ABSTRACT

The Schuster problem has been solved for a stellar atmosphere with spherical symmetry. It is assumed that $l_\rho = c/r^2$, where l_ρ is the line-scattering coefficient, c is a constant, and r is the radius. A table of residual intensity in the line is given for a series of optical thicknesses of the atmosphere. The effect of the sphericity of the stellar atmosphere is to make the cores of the absorption lines, where the optical depth is large, shallower and to make the wings, where the optical depth is small, deeper than for a line formed in a plane-parallel atmosphere.

The interpretation of the observed shapes of lines in supergiants is discussed on the assumption of extended atmospheres for these stars. The effect on line shape of continuous electron scattering in the envelope is briefly considered. The data may also be used to interpret the change in line intensity when a star with an extended atmosphere is eclipsed by a compact body, since the calculations indicate that the fraction of the emergent flux which arises from the scattering in the envelope is appreciable.

1. *Introduction.*—In theoretical discussions of line formation the stellar atmosphere is usually considered to be stratified in parallel planes. However, observations indicate that some stars have a very extensive atmosphere, the extent of the atmosphere being comparable to the radius of the star itself. For such stars the assumption of plane-parallelism is inadequate, and the varying curvature of the outer layers should be allowed for. The purpose of this paper is to solve a simple problem in the theory of line formation for an atmosphere with spherical symmetry and, from a comparison of the results obtained with those obtained for a plane-parallel atmosphere, to estimate the effects of the sphericity of the atmosphere on the line shape.

The Schuster problem in its standard form idealizes the problem of line formation in a stellar atmosphere in the following manner. The photospheric surface emits continuous radiation with an angular distribution specified by

$$I_{ph}(\vartheta) = I_0(1 + \beta \cos \vartheta), \tag{1}$$

where β is related to the coefficient of darkening. Above this surface lies an atmosphere which scatters isotropically with a mass-scattering coefficient, l_ν, which is appreciably different from zero only for a small range of frequencies about the center of the line. For radiation of frequency ν within the line the angular distribution of the intensity emerging from the atmosphere is determined by the solution of the equation of transfer. Integration of this intensity over the outward hemisphere gives the emergent flux, F_ν, in the frequency ν. The ratio of this flux to the flux from the photosphere, F, gives the residual intensity in the line, since the flux in frequencies outside the line is the photospheric flux.

Let the intensity of radiation in frequency ν at depth z in the atmosphere and in a direction ϑ to the outward normal be denoted by $I_\nu(z, \vartheta)$. Then the equation of transfer appropriate to the problem is

$$\cos \vartheta \frac{dI_\nu(z, \vartheta)}{dz} = -l_\nu \rho I_\nu(z, \vartheta) + \tfrac{1}{2} l_\nu \rho \int_0^\pi I_\nu(z, \vartheta') \sin \vartheta' d\vartheta'. \tag{2}$$

The boundary conditions are that there is no incident radiation on the atmosphere at

* This work was completed during tenure of a scholarship from the Canadian Federation of University Women.

$z = z_1$, and that at the base of the atmosphere $z = 0$, where the optical thickness in the frequency ν is

$$\tau_\nu = \int_0^{z_1} l_\nu \rho \, dz , \tag{3}$$

the outward intensity has the value given by equation (1). The emergent flux in frequency ν is

$$F_\nu = 2 \int_0^{\pi/2} I_\nu (0, \vartheta) \sin \vartheta \cos \vartheta \, d\vartheta , \tag{4}$$

and the emergent flux in the continuum is

$$F = 2 \int_0^{\pi/2} I_{ph} (\vartheta) \sin \vartheta \cos \vartheta \, d\vartheta . \tag{5}$$

The ratio of these fluxes gives the residual intensity in the line:

$$R_\nu = \frac{F_\nu}{F} . \tag{6}$$

Chandrasekhar's solution of this problem[1] in his "second approximation" is

$$R_\nu = \frac{1 + \frac{2}{3}\beta\chi(\tau_\nu)}{1.04253 + \frac{2}{3}\beta} \cdot \frac{1}{\chi(\tau_\nu) + \frac{3}{4}\tau_\nu} , \tag{7}$$

where $\chi(\tau_\nu)$ is a certain function of τ_ν and is close to unity.

The Schuster problem in a spherical atmosphere can be formulated similarly. There is a spherical photospheric surface which is surrounded concentrically by an atmosphere extending to infinity. The photosphere emits radiation with an angular distribution that is given by equation (1). The mass-scattering coefficient in the atmosphere is l_ν as before, and the emergent intensity in any frequency ν must be found from the equation of transfer which allows for the curvature of the atmosphere. The residual intensity in the line is found from the ratio of the net emergent flux in the line to the flux in the continuum.

The equation of transfer is

$$\cos \vartheta \frac{\partial I_\nu}{\partial r} - \frac{\sin \vartheta}{r} \frac{\partial I_\nu}{\partial \vartheta} = - l_\nu \rho I_\nu + \tfrac{1}{2} l_\nu \rho \int_0^\pi I_\nu (r, \vartheta') \sin \vartheta' \, d\vartheta' , \tag{8}$$

where r is the distance measured outward from the center of symmetry of the atmosphere and ϑ is the angle measured from the positive direction of the radius vector. This equation must be solved under the boundary conditions that there is no incident radiation on the outside boundary of the atmosphere and that at the base of the atmosphere, where the radial optical depth in frequency ν is

$$\tau_\nu = - \int_\infty^r l_\nu \rho \, dr , \tag{9}$$

the outward intensity equals the photospheric intensity, I_{ph}.

The solution of equation (8) in the "second approximation" for the case $l_\nu \rho \propto r^{-n}$ $(n > 1)$ and under the boundary conditions that all quantities vanish as $r \to \infty$ (this is equivalent in this case to the condition that there is no incident radiation) and that none of the quantities involved increase exponentially as $r \to 0$ has been obtained by Chandrasekhar.[2] The present discussion is based on his work. We shall assume, as he did, that $l_\nu \rho \propto r^{-n} (n > 1)$.

[1] Unpublished.

[2] *Ap. J.*, **101**, 95, 1945. This paper will be referred to as "Paper V."

2. *Solution of the equation of transfer and application of the boundary conditions.*—For the sake of convenience we shall suppress the subscript ν in this part of the discussion. The arguments in Paper V are valid up to the introduction of the boundary conditions. Hence, following the analysis of Paper V, we introduce the abbreviations (cf. Paper V, eqs. [34]–[43]):

$$\begin{aligned} J &= \tfrac{1}{2}\Sigma a_i I_i , & L &= \tfrac{1}{2}\Sigma a_i \mu_i^3 I_i , \\ H &= \tfrac{1}{2}\Sigma a_i \mu_i I_i , & M &= \tfrac{1}{2}\Sigma a_i \mu_i^4 I_i . \\ K &= \tfrac{1}{2}\Sigma a_i \mu_i^2 I_i , \end{aligned} \tag{10}$$

The second approximation is equivalent to the condition

$$35M - 30K + 3J = 0 .$$

Hence the independent quantities are J, H, K, and L. The flux is

$$H = \tfrac{1}{4} F_0 r^{-2} , \tag{11}$$

where F_0 is a constant of integration. After introducing the quantities

$$\begin{aligned} X &= 3K - J , \\ Y &= 5L - 3H , \end{aligned} \tag{12}$$

and expressing all fluxes in units of the emergent flux, F_0/R^2, at the radius R, where $\tau = 1$, we find that the equation of transfer reduces to the pair of simultaneous differential equations (cf. Paper V, eqs. [62] and [63]),

$$\tfrac{7}{3} Y = \frac{dX}{d\tau} + \frac{2}{(n-1)\tau} X \tag{13}$$

and

$$\tfrac{5}{3} X - \frac{1}{(n-1)} \tau^{(3-n)/(n-1)} = \frac{dY}{d\tau} - \frac{4}{(n-1)\tau} Y . \tag{14}$$

Since we assume that $l\rho = cr^{-n} (n > 1)$, it follows from equation (9) that

$$\tau = \frac{c}{n-1} r^{-(n-1)} , \tag{15}$$

where c is a constant.

When the substitutions,

$$z = q\tau \quad \text{with} \quad q = \sqrt{35}/3 = 1.9720$$

and

$$\nu = \frac{n+5}{2(n-1)} , \qquad \mu = \frac{3-n}{2(n-1)} ,$$

are made, it is found that the differential equation to be solved is (cf. Paper V, eq. [70])

$$z^2 \frac{d^2\phi}{dz^2} + z \frac{d\phi}{dz} - (z^2 + \nu^2)\phi = - z^{\mu+1} . \tag{16}$$

If $\phi(z)$ is a solution of equation (16), then it follows that (cf. Paper V, eqs. [71] and [72])

$$X = \frac{7}{3(n-1)} q^{-(n+1)/(n-1)} z^{(n+1)/2(n-1)} \phi(z) \tag{17}$$

and

$$K = q^{-(n+1)/(n-1)} \left[\frac{7}{3(n-1)^2} \int_0^z z^{(3-n)/2(n-1)} \phi(z)\, dz + \frac{n-1}{4(n+1)} z^{(n+1)/(n-1)} \right] . \tag{18}$$

Since the homogeneous part of equation (16) is Bessel's equation for a purely imaginary argument, it can be shown that (cf. Paper V, eq. [80])

$$\phi(z) = I_\nu(z)\int_z^{c_1} z^\mu K_\nu(z)\,dz + K_\nu(z)\int_{c_2}^{z} z^\mu I_\nu(z)\,dz, \tag{19}$$

where $I_\nu(z)$ and $K_\nu(z)$ are the fundamental solutions of this type of Bessel's equation. To satisfy the boundary condition as $r \to \infty$, it is necessary to put $c_2 = 0$, since no quantity may have a singularity at $z = 0$. The constant, c_1, remains arbitrary and must be determined from the other boundary condition of the problem.

In order to do this, we write

$$\phi = \Phi - a\,I_\nu(z), \tag{20}$$

where

$$\Phi = I_\nu(z)\int_z^{\infty} z^\mu K_\nu(z)\,dz + K_\nu(z)\int_0^{z} z^\mu I_\nu(z)\,dz \tag{21}$$

is the function found as a solution in Paper V for an atmosphere of infinite depth, and

$$a = \int_{c_1}^{\infty} z^\mu K_\nu(z)\,dz. \tag{22}$$

The constant a is to be determined from the boundary condition at $z = z_1$.

From equation (17) we have, upon use of equation (20),

$$X = \frac{7}{3(n-1)}\,q^{-(n+1)/(n-1)}\,z^{(n+1)/2(n-1)}\Phi - a\,\frac{7}{3(n-1)}\,q^{-(n+1)/(n-1)}\,z^{(n+1)/2(n-1)}\,I_\nu(z)$$

or

$$X = X_\infty - a\,\frac{7}{3(n-1)}\,q^{-(n+1)/(n-1)}\,z^{(n+1)/2(n-1)}\,I_\nu(z), \tag{23}$$

where

$$X_\infty = \frac{7}{3(n-1)}\,q^{-(n+1)/(n-1)}\,z^{(n+1)/2(n-1)}\Phi$$

is the quantity calculated in Paper V for an infinitely deep atmosphere. The subscript ∞ on any quantity will be used to denote that quantity as it is calculated in Paper V. From equation (18) we find that

$$K = K_\infty - a\beta(z), \tag{24}$$

where

$$\beta(z) = \frac{7}{3(n-1)^2}\,q^{-(n+1)/(n-1)}\int_0^{z} z^{(3-n)/2(n-1)}\,I_\nu(z)\,dz. \tag{25}$$

From equations (12) we then have

$$J = J_\infty - a\gamma(z), \tag{26}$$

where

$$\gamma(z) = 3\beta(z) - \frac{7}{3(n-1)}\,q^{-(n+1)/(n-1)}\,z^{(n+1)/2(n-1)}\,I_\nu(z). \tag{27}$$

From equation (13) we find

$$Y = Y_\infty - a\,\delta(z), \tag{28}$$

where

$$\delta(z) = q^{-2/(n-1)}\,\frac{1}{(n-1)}\left[z^{(n+1)/2(n-1)}\,\frac{dI_\nu(z)}{dz} + \frac{n+5}{2(n-1)}\,z^{[(n+1)/2(n-1)]-1}\,I_\nu(z)\right]. \tag{29}$$

Using the recurrence properties[3] of $I_\nu(z)$, we find

$$\delta(z) = q^{-2/(n-1)} \frac{1}{(n-1)} [\, z^{(n+1)/2(n-1)} I_{\nu-1}(z) \,] . \tag{30}$$

The quantities X, Y, J, and K are expressed in units of F_0/R^2; hence from equation (11) we see that H in the same units is

$$H = \tfrac{1}{4} \left(\frac{R}{r}\right)^2 . \tag{31}$$

In Paper V (cf. eq. [60]) it is shown that

$$\tau = \frac{z}{q} = \left(\frac{R}{r}\right)^{n-1} ;$$

hence it follows that

$$H = \tfrac{1}{4} q^{-2/(n-1)} z^{2/(n-1)} . \tag{32}$$

Since

$$L = \tfrac{1}{5} (Y + 3H) ,$$

we have

$$L = \tfrac{1}{5} [\, Y_\infty + 3H - a\,\delta(z) \,] . \tag{33}$$

The next step is to solve equations (10) for I_{+1} and I_{+2} at $z = z_1$ (z_1 is the radial optical thickness of the atmosphere) and to apply the boundary condition that the outward intensity in the atmosphere at depth z_1 must equal that from the photosphere. We have, since we are working in the "second approximation,"

$$a_1 (I_1 + I_{-1}) + a_2 (I_2 + I_{-2}) - 2J = 0 ,$$

$$a_1\mu_1 (I_1 - I_{-1}) + a_2\mu_2 (I_2 - I_{-2}) - 2H = 0 ,$$

$$a_1\mu_1^2 (I_1 + I_{-1}) + a_2\mu_2^2 (I_2 + I_{-2}) - 2K = 0 ,$$

and

$$a_1\mu_1^3 (I_1 - I_{-1}) + a_2\mu_2^3 (I_2 - I_{-2}) - 2L = 0 ,$$

where we have used the properties of the Gaussian division that $a_i = a_{-i}$ and $u_{-i} = -u_i$. Solution of these four simultaneous equations gives

$$I_1 = \frac{\mu_2^2 (J\mu_1 + H) - (K\mu_1 + L)}{a_1\mu_1 (\mu_2^2 - \mu_1^2)} \tag{34}$$

and

$$I_2 = \frac{-\mu_1^2 (J\mu_2 + H) + (K\mu_2 + L)}{a_2\mu_2 (\mu_2^2 - \mu_1^2)} . \tag{35}$$

These intensities are expressed in units of

$$\frac{F_0}{R^2} = f . \tag{36}$$

[3] Watson, *Treatise on the Theory of Bessel Functions* (Cambridge, England, 1922), p. 79.

When we convert to the usual units and apply the boundary condition at $z = z_1$, we find that

$$\frac{\mu_2^2(J\mu_1+H)-(K\mu_1+L)}{a_1\mu_1(\mu_2^2-\mu_1^2)}=\frac{I_0}{f}(1+\beta\mu_1) \tag{37}$$

and

$$\frac{-\mu_1^2(J\mu_2+H)+(K\mu_2+L)}{a_2\mu_2(\mu_2^2-\mu_1^2)}=\frac{I_0}{f}(1+\beta\mu_2)\,, \tag{38}$$

where the quantities K, J, H, and L are evaluated at $z = z_1$ according to equations (24), (26), (32), and (33).

There are two constants to be determined from the pair of simultaneous equations (37) and (38): a, which is contained in the expression for K, J, and L, and f/I_0. Since the value of these constants depends on z_1, they may be written as $a(z_1)$ and $f(z_1)$. In the case of an infinite atmosphere $a(z_1) = 0$, and $f(z_1)$ is a free parameter; but, for a finite atmosphere, $f(z_1)$ depends on the unknown net flux, for only the outward flux is given and the inward flux (or back-radiation) is determined by the "envelope" which is attached.

The result of substituting the expressions for K, J, H, and L and of solving equations (37) and (38) simultaneously for $a(z_1)$ and $f(z_1)$ is

$$a(z_1)=\frac{\mathfrak{E}(z_1)\,a_1\mu_1(1+\beta\mu_1)+\mathfrak{B}(z_1)\,a_2\mu_2(1+\beta\mu_2)}{\mathfrak{D}(z_1)\,a_1\mu_1(1+\beta\mu_1)+\mathfrak{A}(z_1)\,a_2\mu_2(1+\beta\mu_2)} \tag{39}$$

and

$$f(z_1)=\frac{(\mu_2^2-\mu_1^2)\,[\mathfrak{D}(z_1)\,a_1\mu_1(1+\beta\mu_1)+\mathfrak{A}(z_1)\,a_2\mu_2(1+\beta\mu_2)]}{\mathfrak{B}(z_1)\,\mathfrak{D}(z_1)-\mathfrak{A}(z_1)\,\mathfrak{E}(z_1)}\,, \tag{40}$$

where

$$\mathfrak{A}(z_1)=\mu_1\mu_2^2\gamma(z_1)-\mu_1\beta(z_1)-\tfrac{1}{5}\delta(z_1)\,, \tag{41}$$

$$\mathfrak{D}(z_1)=\mu_1^2\mu_2\gamma(z_1)-\mu_2\beta(z_1)-\tfrac{1}{5}\delta(z_1)\,, \tag{42}$$

$$\mathfrak{B}(z_1)=[\mu_1\mu_2^2J_\infty+(\mu_2^2-\tfrac{3}{5})\,H-\tfrac{1}{5}Y_\infty-\mu_1K_\infty]_{z=z_1}\,, \tag{43}$$

and

$$\mathfrak{E}(z_1)=[\mu_1^2\mu_2J_\infty+(\mu_1^2-\tfrac{3}{5})\,H-\tfrac{1}{5}Y_\infty-\mu_2K_\infty]_{z=z_1}\,. \tag{44}$$

(The function $\beta(z)$, defined in eq. [25], should not be confused with the constant β, which depends on the coefficient of darkening of the photosphere.)

For any value of the coefficient of darkening of the photosphere a series of $a(z_1)$ and $f(z_1)$ can be calculated from equations (39) and (40) for selected values of z_1, the total optical thickness of the envelope for radiation of any given frequency. Once $a(z_1)$ is known, the source function $J(z)$ may be found from equation (26) for any optical depth $z \leq z_1$ in the atmosphere. Table 1 gives the quantities $a(z_1)$ and $f(z_1)$ when $\beta = 2$.

3. *The formation of lines.*—In order to find the residual intensity at any frequency ν, it is necessary to find the emergent flux in that frequency. In the Schuster problem each frequency of radiation is characterized by a unique total optical thickness of the atmosphere. We have

$$l_\nu\rho=\frac{c_\nu}{r^n}\,, \tag{45}$$

where c is a constant for any frequency. The variation of c with ν corresponds to the variation of the scattering coefficient with ν. In the following discussion it is assumed that the variation of l_ν with frequency is constant with depth, making the discussion the same for all frequencies, hence the suffix ν may be suppressed. The case with $n = 2$ will be studied. Then

$$l\rho = \frac{c}{r^2}. \tag{46}$$

The adoption of $n = 2$ gives a fairly steep gradient for the scattering coefficient, for, if at $r = r_1$, $l\rho$ has a given value, at $2r_1$ it will have one-quarter this value, at $3r_1$, one-ninth this value, and so on. For the case[4] in which ρ varies as r^{-2}, it means that l, the scattering coefficient per atom, is independent of r. How true this is in an actual star depends on the variation of temperature and pressure with radius, and hence of the ionization and excitation equilibria. Although the radius of the star is allowed to extend

TABLE 1

THE CONSTANTS $a(z_1)$ AND $f(z_1)$

z_1	$a(z_1)$	$f(z_1)$	z_1	$a(z_1)$	$f(z_1)$
0.0	.....	.....	1.6	2.19883	0.54190
0.1	9925.773	11.02985	1.8	1.48005	.47068
0.2	1267.721	5.40606	2.0	1.02960	.41462
0.3	358.8193	4.02397	2.2	0.73517	.36949
0.4	159.98997	2.60939	2.4	0.57907	.33398
0.5	82.02384	2.04822	2.6	0.39761	.30188
0.6	47.38368	1.67583	2.8	0.29933	.27548
0.7	29.47683	1.42230	3.0	0.22817	.25322
0.8	19.76638	1.21408	3.5	0.12043	.20949
0.9	13.85398	1.04572	4.0	0.06645	.17763
1.0	9.92324	0.94072	4.5	0.03774	.15343
1.2	5.59178	0.76119	5.0	0.02192	.13448
1.4	3.40860	0.63800	5.5	0.01293	0.11924

to infinity, it is seen that with $n = 2$ the effective atmosphere in which $l\rho$ is significantly large is not exorbitantly extended.

The emergent flux from a spherical atmosphere is

$$F = 2\pi \int_0^\infty p I(p)\, dp, \tag{47}$$

where $I(p)$ is the emergent intensity along a line OA at a perpendicular distance p from the center of the star (see Fig. 1). The quantity p varies from 0 to ∞, since the radius of the star extends to infinity. If $I(\theta, p)$ refers to the intensity of radiation at a point P on the line OA, then, quite generally,[5]

$$I(\theta, p) = e^{p\int_0^\theta l\rho \operatorname{cosec}^2\theta d\theta} \int_0^{\theta_1} e^{-p\int_0^\varphi l\rho \operatorname{cosec}^2\varphi d\varphi} J(\varphi, p)\, pl\rho \operatorname{cosec}^2\varphi\, d\varphi, \tag{48}$$

where $J(\varphi, p)$ is the source function at a point on OA characterized by the angle φ and θ_1 is the maximum angle that φ can reach. In our case we have a photosphere of radius r_1; hence when $p > r_1$, θ_1 is π; when $p \leq r_1$, θ_1 is $\sin^{-1} p/r_1$. To obtain the emergent intensity, we must set $\theta = 0$.

[4] Cf. N. A. Kosirev, *M.N.* **94**, 430, 1934.

[5] S. Chandrasekhar, *Proc. Cambridge Phil. Soc.* **31**, 390, 1935.

Thus for all $p > r_1$ the emergent intensity arising from light scattered in the envelope is

$$I_1(p) = \left[\int_0^{\pi} e^{-p\int_0^{\varphi} l\rho \operatorname{cosec}^2 \varphi d\varphi} J(\varphi, p)\, pl\rho \operatorname{cosec}^2 \varphi d\varphi\right]_{p>r_1}, \tag{49}$$

while for all $p \leq r_1$ it is

$$I_2(p) = \left[\int_0^{\sin^{-1} p/r_1} e^{-p\int_0^{\varphi} l\rho \operatorname{cosec}^2 \varphi d\varphi} J(\varphi, p)\, pl\rho \operatorname{cosec}^2 \varphi d\varphi\right]_{p\leq r_1}. \tag{50}$$

For all $p \leq r_1$ there is also an emergent intensity arising from the transmitted light of the photosphere. This is

$$I_3(p) = e^{-p\int_0^{\theta_1} l\rho \operatorname{cosec}^2 \varphi d\varphi} I_0(1 + \beta \cos \theta_1) \tag{51}$$

where

$$\theta_1 = \sin^{-1} \frac{p}{r_1}. \tag{52}$$

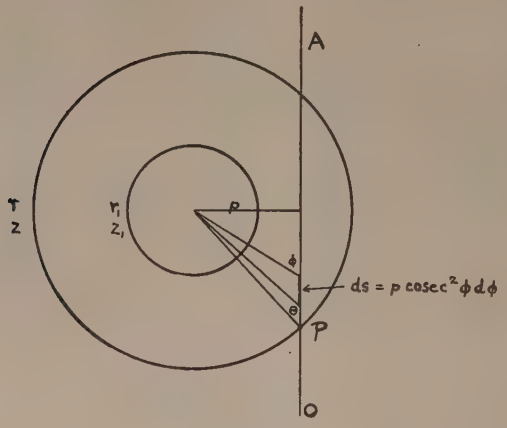

FIG. 1

In equations (49), (50), and (51) $l\rho$ is a function of p and φ, for

$$l\rho = \frac{c}{r^2} = \frac{c}{p^2 \operatorname{cosec}^2 \varphi}. \tag{53}$$

The introduction of equation (53) into equations (49), (50), and (51) gives

$$I_1(p) = \frac{c}{p}\int_0^{\pi} e^{-c\varphi/p} J(\varphi, p)\, d\varphi, \tag{54}$$

$$I_2(p) = \frac{c}{p}\int_0^{\sin^{-1} p/r_1} e^{-c\varphi/p} J(\varphi, p)\, d\varphi, \tag{55}$$

and

$$I_3(p) = e^{-c\theta_1/p} I_0(1 + \beta \cos \theta_1). \tag{56}$$

The net flux in any frequency of the line is then given by

$$F_\nu = 2\pi\int_{r_1}^{\infty} p\, I_1(p)\, dp + 2\pi\int_0^{r_1} p\, I_2(p)\, dp + 2\pi\int_0^{r_1} p\, I_3(p)\, dp. \tag{57}$$

Let F_1, F_2, and F_3 be, respectively, the first, second, and third parts of F_ν. The dependence on frequency of each of these fluxes is given by the constant, c, which enters the expressions for $I_1(p)$, $I_2(p)$, and $I_3(p)$.

The flux from the photosphere is

$$F = 2\pi r_1^2 I_0 \int_0^{\pi/2} (1+\beta\cos\theta)\sin\theta\cos\theta\, d\theta\,, \tag{58}$$

which gives us

$$F = 2\pi r_1^2 I_0 (\tfrac{1}{2}+\tfrac{1}{3}\beta)\,. \tag{59}$$

Accordingly, we find that the residual intensity in the line is

$$R_\nu = \frac{F_\nu}{F} = R_1 + R_2 + R_3\,, \tag{60}$$

where

$$R_1 = \frac{F_1}{F}, \qquad R_2 = \frac{F_2}{F}, \qquad \text{and} \qquad R_3 = \frac{F_3}{F}. \tag{61}$$

The fluxes F_1, F_2, and F_3 must be evaluated explicitly as functions of z_1, the total optical thickness of the atmosphere in radiation of frequency ν.

Let

$$p = \xi r_1\,. \tag{62}$$

Then, after some simple substitutions, we find that

$$R_1 = \frac{z_1}{I_0(\frac{1}{2}+\frac{1}{3}\beta)\,q}\int_1^\infty d\xi \int_0^\pi e^{-z_1\varphi/q\xi} J(\varphi,\xi)\, d\varphi \tag{63}$$

and

$$R_2 = \frac{z_1}{I_0(\frac{1}{2}+\frac{1}{3}\beta)\,q}\int_0^1 d\xi \int_0^{\sin^{-1}\xi} e^{-z_1\varphi/q\xi} J(\varphi,\xi)\, d\varphi\,. \tag{64}$$

The source function $J(\varphi, \xi)$ is evaluated at the point characterized by the co-ordinates φ and ξ. Since

$$z = q\tau = \frac{z_1 r_1}{c}\cdot\frac{c}{r},$$

we have

$$z = z_1 \frac{\sin\varphi}{\xi} \tag{65}$$

hence any pair of values of φ and ξ characterize an optical depth, z, thus:

$$J(\varphi,\xi) \equiv J(z)\,. \tag{66}$$

We have shown in equation (26) how to calculate the source function, $J(z)$, in units of $I_0 f(z_1)$. Equation (40) enables us to calculate the quantity $f(z_1)$; hence, in the usual units,

$$J(\varphi,\xi) \equiv I_0 f(z_1)\, J(z)\,. \tag{67}$$

When we substitute this expression for $J(\varphi, \xi)$ in equations (63) and (64), we find that

$$R_1 = \frac{z_1}{q}\frac{f(z_1)}{(\frac{1}{2}+\frac{1}{3}\beta)}\int_1^\infty d\xi \int_0^\pi e^{-z_1\varphi/q\xi} J(z)\, d\varphi \tag{68}$$

and

$$R_2 = \frac{z_1}{q}\frac{f(z_1)}{(\frac{1}{2}+\frac{1}{3}\beta)}\int_0^1 d\xi \int_0^{\sin^{-1}\xi} e^{-z_1\varphi/q\xi} J(z)\, d\varphi\,. \tag{69}$$

The expression for R_3 is

$$R_3 = \frac{\int_0^{r_1} p\, e^{-c\theta_1/p}\,(1+\beta\cos\theta_1)\,dp}{r_1^2\,(\frac{1}{2}+\frac{1}{3}\beta)}. \tag{70}$$

Since $p = r_1 \sin\theta_1$, we shall transform to the variable θ_1; we also note that $c/r_1 = z_1/q$. Then we have

$$R_3 = (\tfrac{1}{2}+\tfrac{1}{3}\beta)^{-1}\int_0^{\pi/2} e^{-z_1\theta_1/q\sin\theta_1}\,(1+\beta\cos\theta_1)\sin\theta_1\cos\theta_1 d\theta_1. \tag{71}$$

Referring to equations (68), (69), and (71), we see that the residual intensity, $R_\nu = R_1 + R_2 + R_3$, can be found explicitly if the quantity z_1 is known. This solves the Schuster problem in a spherical atmosphere.

4. *Numerical work.*—According to equation (26),

$$J(z) = J_\infty(z) - a(z_1)\,\gamma(z).$$

In Paper V we saw that (cf. eq. [83]), for the case $n = 2$,

$$J_\infty(z) = q^{-3}[\tfrac{1}{4}z^3 + \Delta_\infty(z)], \tag{72}$$

where

$$\Delta_\infty(z) = [J_\infty(z)]_{\text{2d approx}} - [J_\infty(z)]_{\text{1st approx}}. \tag{73}$$

The quantity $\Delta_\infty(z)$ can be evaluated numerically from the tables in Paper V. If we write the source function as

$$q^3 J(z) = \tfrac{1}{4}z^3 + \epsilon(z, z_1), \tag{74}$$

where

$$\epsilon(z, z_1) = \Delta_\infty(z) - a(z_1)\,q^3\gamma(z), \tag{75}$$

and substitute equation (74) in equations (68) and (69), we find that

$$R_1 = \frac{z_1}{q^4}\frac{f(z_1)}{(\frac{1}{2}+\frac{1}{3}\beta)}[\Im_1' + \Im_2''] \tag{76}$$

and

$$R_2 = \frac{z_1}{q^4}\frac{f(z_1)}{(\frac{1}{2}+\frac{1}{3}\beta)}[\Im_2' + \Im_2''], \tag{77}$$

where

$$\Im_1' = \frac{1}{4}\int_1^\infty d\xi \int_0^\pi d\varphi\, e^{-z_1\varphi/q\xi} z^3, \tag{78}$$

$$\Im_1'' = \int_1^\infty d\xi \int_0^\pi d\varphi\, e^{-z_1\varphi/q\xi}\epsilon(z, z_1), \tag{79}$$

$$\Im_2' = \frac{1}{4}\int_0^1 d\xi \int_0^{\sin^{-1}\xi} d\varphi\, e^{-z_1\varphi/q\xi} z^3, \tag{80}$$

and

$$\Im_2'' = \int_0^1 d\xi \int_0^{\sin^{-1}\xi} d\varphi\, e^{-z_1\varphi/q\xi}\epsilon(z, z_1). \tag{81}$$

The integrals $\Im_1''$ and $\Im_2''$ may be neglected, since $\epsilon(z, z_1)$ is small compared to $\frac{1}{4}z^3$. Some typical values of $\epsilon(z, z_1)$ are given in Table 2. Although, with large z, $\epsilon(z, z_1)$ becomes comparable to $\frac{1}{4}z^3$, the product $\epsilon(z, z_1)\exp(-z_1\varphi/q\xi)$, which enters the integrals

$\mathfrak{I}_1''$ and $\mathfrak{I}_2''$, always remains small, for equation (65) shows that, for any given z_1/q and ξ, the term $z_1\varphi/q\xi$ increases with increasing z. The neglect of $\mathfrak{I}_1''$ and $\mathfrak{I}_2''$ means that we are using the source function in the first approximation.

The integral $\mathfrak{I}_1'$ may be evaluated as follows: From equations (65) and (78) we have

$$\mathfrak{I}_1' = \tfrac{1}{4} z_1^3 \int_1^\infty d\xi \int_0^\pi d\varphi \, e^{-z_1\varphi/q\xi} \frac{\sin^3 \varphi}{\xi^3}. \tag{82}$$

If we put $z_1\varphi/q = a$ and invert the order of integration, we obtain

$$\mathfrak{I}_1' = \tfrac{1}{4} z_1^3 \int_0^\pi d\varphi \sin^3 \varphi \int_1^\infty d\xi \, e^{-a/\xi} \xi^{-3}. \tag{83}$$

TABLE 2

TYPICAL $\epsilon(z, z_1)$

z	$\frac{1}{4}z^3$	$\epsilon(z, z_1)$		z	$\frac{1}{4}z^3$	$\epsilon(z, z_1)$
		$z_1 = 1$	$z_1 = 5$			$z_1 = 5$
0.0	0.0000000	0.0000000	0.0000000	1.6	1.02400	0.08322
0.1	.0002500	.0000008	.0000000	1.8	1.45800	0.13100
0.2	.0020000	.0000323	.0000097	2.0	2.0000	0.1973
0.3	.0067500	.0002372	.0000658	2.2	2.6620	0.2781
0.4	.016000	.000967	.000240	2.4	3.4560	0.3827
0.5	.031250	.002881	.000645	2.6	4.3940	0.5112
0.6	.054000	.007044	.001432	2.8	5.4880	0.6667
0.7	.085750	.013699	.002789	3.0	6.7500	0.8524
0.8	.12800	.02910	.00493	3.5	10.7188	1.4760
0.9	.18225	.05224	.00811	4.0	16.0000	2.4060
1.0	.25000	0.08843	.01258	4.5	22.7813	3.8246
1.2	.43200	.....	.02656	5.0	31.2500	6.0446
1.4	0.68600	.....	0.04926			

Then we make the substitution $x = 1/\xi$ and evaluate the integral over x, getting

$$\mathfrak{I}_1' = \tfrac{1}{4} z_1^3 \int_0^\pi d\varphi \sin^3 \varphi a^{-2} [1 - e^{-a}(a+1)]. \tag{84}$$

We then replace a by $z_1\varphi/q$ and substitute $\mu = \cos\varphi$, which gives us

$$\mathfrak{I}_1' = \frac{q^2 z_1}{4} \int_{-1}^{+1} d\mu (1-\mu^2) \left\{ \frac{1}{\varphi^2} - \frac{1}{\varphi^2} e^{-z_1\varphi/q} - \frac{z_1}{q\varphi} e^{-z_1\varphi/q} \right\}. \tag{85}$$

This integral may be evaluated numerically by using Gauss's quadrature formula; thus,

$$\mathfrak{I}_1' = \frac{q^2 z_1}{4} \left[\sum_{j=-n}^{+n} \frac{a_j}{\varphi_j^2}(1-\mu_j^2) - \sum_{j=-n}^{+n} \frac{a_j}{\varphi_j^2}(1-\mu_j^2) e^{-z_1\varphi_j/q} - \frac{z_1}{q} \sum_{j=-n}^{+n} \frac{a_j}{\varphi_j}(1-\mu_j^2) e^{-z_1\varphi_j/q} \right], \tag{86}$$

where the a_j's are Gaussian weights,[6] the μ_j's are the roots of Legendre polynomial of order $2n+1$, and the summation is carried out over both positive and negative roots. Also we have

$$\varphi_j = \cos^{-1} \mu_j. \tag{87}$$

[6] *Bull. Am. Math. Soc.*, 48, 741, 1942.

A five-point formula, j running from -2 to $+2$, was found to yield sufficiently accurate results.

The integral $\mathfrak{I}_2'$ is evaluated in a similar manner. We have

$$\mathfrak{I}_2' = \frac{z_1^3}{4} \int_0^1 d\xi \int_0^{\sin^{-1}\xi} d\varphi \, e^{-z_1\varphi/q\xi} \frac{\sin^3 \varphi}{\xi^3}. \tag{88}$$

If we invert the order of integration and substitute $a = z_1\varphi/q$, we obtain

$$\mathfrak{I}_2' = \frac{z_1^3}{4} \int_0^{\pi/2} d\varphi \, \sin^3 \varphi \int_{\sin\varphi}^1 d\xi \, e^{-a/\xi} \xi^{-3}. \tag{89}$$

The integral over ξ is evaluated as in the previous case, with the result that

$$\mathfrak{I}_2' = \frac{z_1^3}{4} \int_0^{\pi/2} d\varphi \, \sin^3 \varphi a^{-2} \left[e^{-a}(a+1) - e^{-a/\sin\varphi} \left(\frac{a}{\sin\varphi} + 1 \right) \right]. \tag{90}$$

Then a is replaced by $z_1\varphi/q$, the terms are collected, and $\mu = \cos\varphi$ is introduced, giving us

$$\mathfrak{I}_2' = \frac{q^2 z_1}{4} \int_0^1 d\mu \, (1-\mu^2) \left[\frac{1}{\varphi^2} \{ e^{-z_1\varphi/q} - e^{-z_1\varphi/q(1-\mu^2)^{1/2}} \} + \frac{z_1}{q\varphi} \{ e^{-z_1\varphi/q} - (1-\mu^2)^{-1/2} e^{-z_1\varphi/q(1-\mu^2)^{1/2}} \} \right]. \tag{91}$$

We again evaluate this integral by Gauss's formula, the roots of a Legendre polynomial of order $2n$ being now used and the summation being extended over the positive j-values. Thus we get

$$\mathfrak{I}_2' = \frac{q^2 z_1}{4} \left[\sum_{j=1}^{n} \frac{a_j}{\varphi_j^2} (1-\mu_j^2) \{ e^{-z_1\varphi_j/q} - e^{-z_1\varphi_j/q(1-\mu^2)^{1/2}} \} + \frac{z_1}{q} \sum_{j=1}^{n} \frac{a_j}{\varphi_j} (1-\mu_j^2) \{ e^{-z_1\varphi_j/q} - (1-\mu_j^2)^{-1/2} e^{-z_1\varphi_j/q(1-\mu_j^2)^{1/2}} \} \right]. \tag{92}$$

A five-point formula—$j = 1, 2, 3, 4, 5$—is used.

Let the integral in the expression for R_3 (eq. [70]) be $\mathfrak{I}_3$, then

$$\mathfrak{I}_3 = \int^{\pi/2} e^{-z_1\theta_1/q \sin\theta_1} (1 + \beta \cos\theta_1) \sin\theta_1 \cos\theta_1 d\theta_1. \tag{93}$$

Let $\mu = \cos\theta_1$, and evaluate the integral by an even Gaussian division, as for integral $\mathfrak{I}_2'$. Then we have

$$\mathfrak{I}_3 = \sum_{j=1}^{n} a_j \mu_j (1 + \beta\mu_j) \exp\left[-\frac{z_1\theta_j}{q(1-\mu_j^2)^{1/2}} \right]. \tag{94}$$

It is sufficient to use a five-point formula.

Table 3 gives R_1, R_2, R_3, and R, calculated according to equations (68), (69), and (71) for various values of z_1, and hence of τ_1, the total optical thickness of the atmosphere for radiation of frequency ν. Table 4 gives a table of residual intensities for a plane-parallel Schuster atmosphere calculated according to equation (7).

Evaluation of the integrals $\mathfrak{I}_1''$ and $\mathfrak{I}_2''$ will increase the values of R_1 and R_2 by a few per cent. In view of the uncertainty with which our idealized model fits a real star, it does not seem worth while to evaluate $\mathfrak{I}_1''$ and $\mathfrak{I}_2''$.

TABLE 3

SPHERICAL ATMOSPHERE

z_1	$\tau_1 = z_1/q$	R_1	R_2	R_3	R
0.0	0.0000	0.0000	0.0000	1.0000	1.0000
0.1	0.0507	.0018	.0004	0.9479	0.9501
0.2	0.1014	.0065	.0022	0.8957	0.9044
0.3	0.1521	.0155	.0039	0.8462	0.8656
0.4	0.2028	.0228	.0058	0.7997	0.8283
0.5	0.2536	.0332	.0085	0.7556	0.7973
0.6	0.3043	.0444	.0114	0.7140	0.7698
0.7	0.3550	.0570	.0147	0.6747	0.7464
0.8	0.4057	.0692	.0180	0.6376	0.7248
0.9	0.4564	.0809	.0210	0.6025	0.7044
1.0	0.5071	.0935	.0248	0.5694	0.6877
1.2	0.6085	.1214	.0318	0.5086	0.6618
1.4	0.7099	.1470	.0384	0.4544	0.6398
1.6	0.8114	.1715	.0448	0.4059	0.6222
1.8	0.9128	.1947	.0508	0.3627	0.6082
2.0	1.0142	.2165	.0562	0.3241	0.5968
2.2	1.1156	.2368	.0611	0.2896	0.5875
2.4	1.2170	.2567	.0658	0.2589	0.5814
2.6	1.3185	.2731	.0694	0.2314	0.5739
2.8	1.4199	.2887	.0725	0.2069	0.5681
3.0	1.5213	.3032	.0753	0.1849	0.5634
3.5	1.7748	.3341	.0802	0.1398	0.5541
4.0	2.0284	.3584	.0826	0.1058	0.5468
4.5	2.2819	.3770	.0829	0.0800	0.5399
5.0	2.5355	.3913	.0817	0.0606	0.5336
5.5	2.7890	0.4018	0.0794	0.0459	0.5271

TABLE 4

PLANE-PARALLEL ATMOSPHERE

τ_1	R	τ_1	R	τ_1	R	τ_1	R
0.00	1.000	0.35	0.7780	0.90	0.5859	2.00	0.3954
.05	0.9588	.40	.7547	1.00	.5612	2.20	.3734
.10	0.9219	.50	.7129	1.20	.5176	2.40	.3538
.15	0.8888	.60	.6760	1.40	.4804	2.60	.3360
.20	0.8576	.70	.6428	1.60	.4483	2.80	.3200
.25	0.8285	0.80	0.6127	1.80	0.4202	3.00	0.3055
0.30	0.8024						

5. *Discussion of the results.*—Figure 2 gives the data of Tables 3 and 4 plotted against τ_1. For very small τ_1—$\tau_1 < 0.05$—the two curves are practically identical, as might be expected, since for very small τ_1 the effect of the curvature of the atmosphere will be negligible. For $0.05 < \tau_1 < 0.8$ the residual intensity in the plane-parallel atmosphere is greater than that in the spherical atmosphere. For $\tau_1 > 0.8$ the residual intensity in the spherical atmosphere becomes greater than that in the plane-parallel atmosphere. The effect of this is shown in Figure 3, which gives line profiles calculated for a spherical

Schuster atmosphere and for a plane-parallel Schuster atmosphere. Figure 3, *a*, is obtained when it is assumed that $\tau = \tau_0 e^{-(\Delta\lambda)^2}$, Figure 3, *b*, when $\tau = \tau_0[1 + (\Delta\lambda)^2]^{-1}$. In both cases the same $\tau_0 = 2.7890$ was used. The following conclusions are evident from inspection of the line profiles:

1. The cores of the lines are blunter and more shallow in a spherical atmosphere than in a plane-parallel atmosphere.
2. The wings of the lines are deeper in a spherical atmosphere than in a plane-parallel atmosphere.
3. When the absorption coefficient has a Gaussian form (Fig. 3, *a*), the equivalent width of the line formed in the spherical atmosphere is less than that of the line formed in a plane-parallel atmosphere.

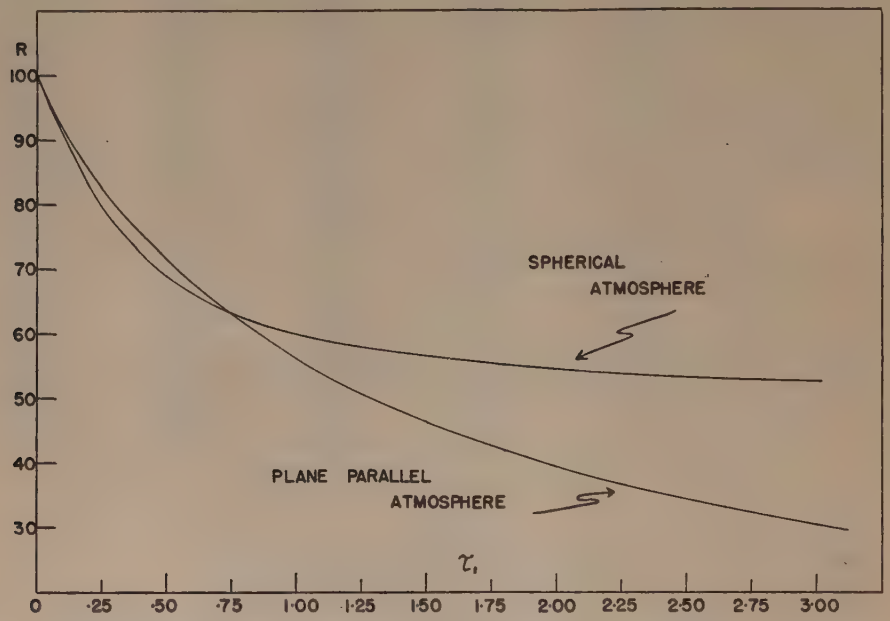

FIG. 2.—The variation of residual intensity with τ_1 for a spherical and a plane-parallel atmosphere. R is given in percentage of the continuum.

4. When the absorption coefficient has a damping form (Fig. 3, *b*), the equivalent width in the two cases may remain much the same, as the reduction in equivalent width caused by the shallowing of the core of the line formed in a spherical atmosphere is largely compensated by the deepening of the extensive wings of this line.

The most significant result of the curvature of the atmosphere is that, for $\tau_1 > 2$, the residual intensity in the spherical atmosphere is much greater than that in the plane-parallel atmosphere. Thus the cores of the lines formed in a spherical atmosphere will be shallower than those of lines formed in a plane-parallel atmosphere. This effect might be observed in some lines of supergiant stars. For the elements other than *H* or *He*, τ_0 is not very large and may fall in the range of values in Tables 3 and 4. If this is true and the curvature of the atmosphere is important for supergiants, the lines in supergiants should have blunter, shallower cores than the lines in main-sequence stars. However, rotation and mass motion of the atmosphere also shallow the lines. Thus it may be dif-

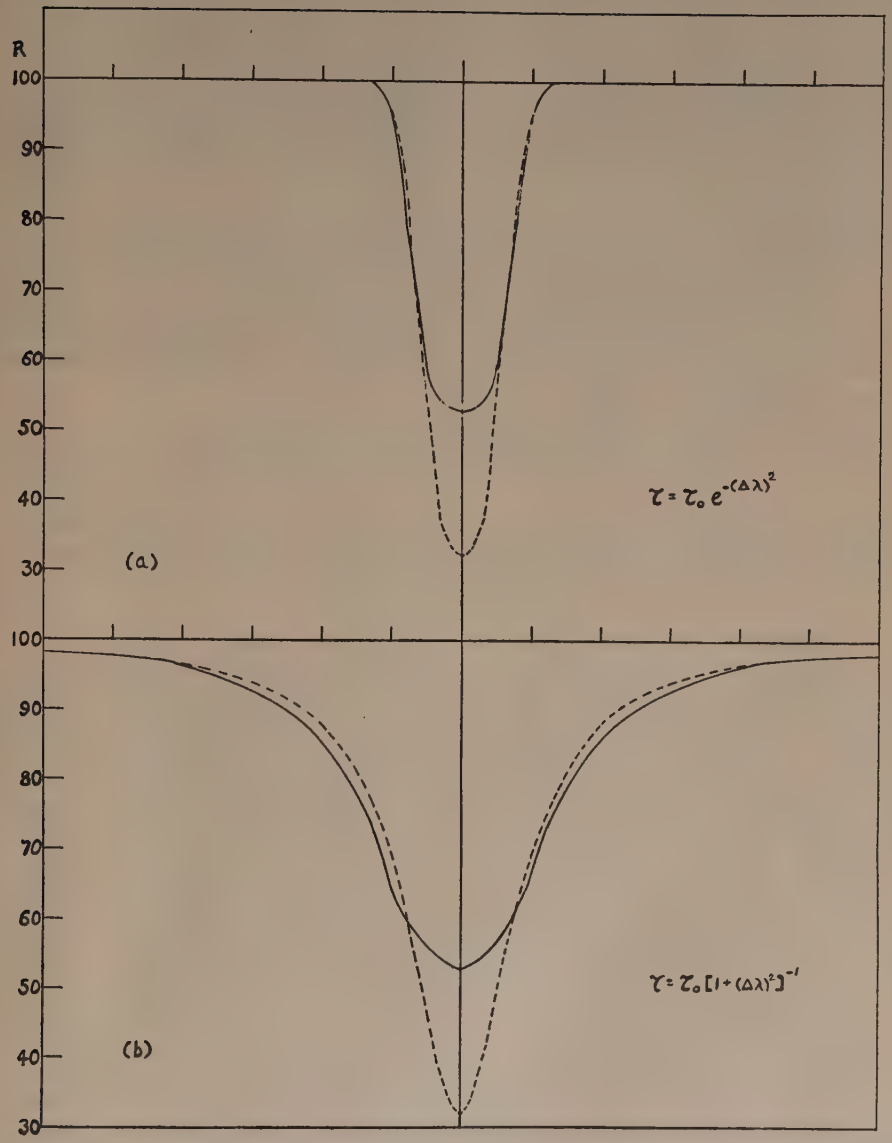

FIG. 3.—Line shapes in a spherical and a plane-parallel atmosphere, (*a*) when the absorption coefficient has Gaussian form, (*b*) when the absorption coefficient has damping form. The solid curve gives the profile in a spherical atmosphere; the broken curve gives the profile in a plane-parallel atmosphere. The residual intensity is given in percentage of the continuum. The wave-length scale is arbitrary.

ficult to interpret shallow lines in supergiants directly as a result of sphericity. Although rotation of the star broadens the lines, it does not change their relative equivalent widths. Uniform mass motion of the atmosphere causes displacements of the lines (which will be difficult to separate from the peculiar motion of the star except when there is some outside indication of the star's true radial velocity) and may also cause certain asymmetries of all lines.[7] On the other hand, the shallowing effects of the sphericity of the atmosphere depend greatly upon the strength of the line, that is upon τ_0. Only for $\tau_0 > 2$ will the shallowing of the cores be conspicuous. Thus a comparison of strong and weak lines in supergiant and main-sequence stars may reveal the effects of the sphericity of the atmosphere.

If a similar comparison is to be made for the hydrogen lines, the tables must be extended to larger values of τ_1. The following asymptotic form for R results if only the terms with the highest power of z are included in the expression for $f(z_1)$ (see eq. [40]) and if only the first term in the integral $\mathfrak{I}_1'$ is used (see eq. [86]). The figures in Table 3 show that the integrals $\mathfrak{I}_2'$ and $\mathfrak{I}_3$, which give R_2 and R_3, become negligible with increasing z. Furthermore, the computations show that, with large z, only the first term in the integral $\mathfrak{I}_1'$ is significant. We find

$$R\,(\text{large } z_1) = \frac{(\mu_2^2-\mu_1^2)}{(\frac{1}{2}+\frac{1}{3}\beta)} \frac{[a_1\mu_1(1+\beta\mu_1)+a_2\mu_2(1+\beta\mu_2)]}{[\frac{1}{4}(\mu_1\mu_2^2-\mu_2\mu_1^2)-\frac{1}{12}(\mu_1-\mu_2)]} \frac{1}{4}\frac{q}{z_1}\sum_j a_j(1-\mu_j^2)\frac{1}{\theta_j^2}, \quad (95)$$

where the summation over j is carried out over the zeros of a Legendre polynomial of odd order. When the appropriate numerical values are introduced, we obtain

$$R\,(\text{large } z_1) = \frac{5.587}{\tau_1}, \quad (96)$$

where q/z_1 has been replaced by τ_1, according to the definition of τ_1. Equation (7) may still be used to give the residual intensity for large τ_1 in a plane-parallel atmosphere. The use of equations (96) and (7) gives us the values shown in Table 5.

We see that, for large τ_1 also, the residual intensity in a spherical atmosphere is larger than the residual intensity in a plane-parallel atmosphere. However, the detection of this difference from observations would require very careful photometry. If the curvature of the atmosphere is important in the formation of the hydrogen lines of supergiants, the line profiles for these stars should show sharp, deep cores with comparatively high "shoulders," since, according to Table 3, the residual intensity in the "shoulders" of the lines, where τ_1 might be of the order of 2 or 3, will be considerably higher than for lines formed in a plane-parallel atmosphere. The comparisons which are discussed above assume that the Schuster idealization represents the formation of lines in main-sequence and in supergiant stars. Although such an assumption may not be justified, it is probable that the main features of the argument would carry over if a more detailed theory of line formation were used.

If the sphericity of the atmosphere is important in determining the line shape in supergiants, the change in equivalent width that may ensue will have an important effect on the curve of growth. Consideration of the variation of R with τ_1 in Tables 3 and 4 and of Figure 3 leads to the following conclusions. If the line is very weak, i.e., τ_0 small, the equivalent width will be somewhat larger in a spherical atmosphere than in a plane-parallel atmosphere. For such lines $\log W/\lambda \propto N$ would likely be true. As τ_0 increases, the absorption coefficient being still predominantly Gaussian in form, the case of Figure 3, *a*, is reached. Then W in the spherical atmosphere is less than W in the plane-parallel atmosphere; hence the curve of growth for such a star will begin to flatten out sooner than it would for a star with a plane-parallel atmosphere. However, in the

[7] *Ap. J.*, 106, 128, 1947.

supergiant stars turbulence is important and tends to lift the flat part of the curve of growth,[8] the line-absorption coefficient remaining Gaussian in form. The net result of the opposing effects of sphericity and turbulence will be to show a reduced lifting of the flat portion of the curve of growth. Hence a smaller turbulent velocity than is actually the case will be deduced. The damping portion of the curve of growth might remain much the same in a spherical and plane-parallel atmosphere, since Figure 3, *b*, shows that, when the absorption coefficient has a damping form, there may be little difference in equivalent width between the two cases.

TABLE 5

RESIDUAL INTENSITIES FOR LARGE τ_1

τ_1	Spherical Atmosphere R	Plane-parallel Atmosphere R
50	0.112	0.026
100	.056	.013
1000	0.006	0.001

TABLE 6

THE EFFECT OF CONTINUOUS SCATTERING IN THE ATMOSPHERE*

$z_{1\nu}$	Spherical Atmosphere			Plane-parallel Atmosphere		
	$z_{1\sigma}=0.0$	$z_{1\sigma}=0.1$	$z_{1\sigma}=2.0$	$z_{1\sigma}=0.0$	$z_{1\sigma}=0.1$	$z_{1\sigma}=2.0$
0.0	1.000	1.000	1.000	1.000	1.000	1.000
0.2	0.904	0.911	0.983	0.921	0.926	0.960
0.4	0.828	0.839	0.974	0.856	0.863	0.920
0.6	0.770	0.785	0.961	0.800	0.810	0.888
0.8	0.725	0.741	0.952	0.752	0.763	0.854
1.0	0.688	0.711	0.943	0.710	0.722	0.826
2.0	0.597	0.623	0.916	0.558	0.571	0.703
3.0	0.563	0.585	0.895	0.461	0.473	0.612
4.0	0.547	0.570	.....	0.393	0.405	.....
5.0	0.534	0.556	.....	0.342	0.352	.....

* The table gives R'_ν.

These remarks emphasize again the necessity of the study of line profiles in supergiant stars rather than deriving information from curves of growth only, since so many opposing tendencies, whose effects are obliterated in a mere study of equivalent widths, may be at work.

From Tables 3 and 4 we can also estimate the effect of the occurrence of continuous scattering in the atmosphere, as well as line scattering. Such scattering might arise from the presence of electrons. The continuous scattering coefficient, σ, is independent of frequency. Let the optical depth in the atmosphere due to continuous scattering be τ_σ. Then the flux emerging from the atmosphere in frequencies outside a line is

$$F_c = R(\tau_\sigma) F , \qquad (97)$$

[8] *Ap. J.*, **79**, 409, 1934.

where F is the photospheric flux. The emergent flux for any frequency in the line is

$$F_\nu = R(\tau_\sigma + \tau_\nu) F , \tag{98}$$

where τ_ν is the optical thickness of an atmosphere without continuous scattering for radiation of frequency ν; hence $\tau_\sigma + \tau_\nu$ is the total optical thickness in the frequency ν. The residual intensity of the line will be

$$R'_\nu = \frac{F_\nu}{F_c} = \frac{R(\tau_\sigma + \tau_\nu)}{R(\tau_\sigma)} . \tag{99}$$

Table 6 gives the results for a spherical and a plane-parallel atmosphere when the optical depth due to electron scattering corresponds to $z_{1\sigma} = 0, 0.1$, and 2.0. The residual intensity is calculated according to equation (99) for a series of total optical depths $z_{1\sigma} + z_{1\nu}$ corresponding to the values of $z_{1\nu}$ given in the first column. We see that the effect of superposed electron scattering is to shallow the line in all cases, the effects of electron scattering being enhanced in a spherical atmosphere.

Table 3 offers an interesting opportunity for considering possible line-intensity changes during the eclipse of an extended star by a dark or faintly luminous compact body. The quantity R_1 is the part of the residual intensity in the line arising from the integrated flux over all the envelope except that part immediately in front of the disk; R_2 is the part of the residual intensity in the line arising from that part of the envelope in front of the disk; R_3 is the part of the residual intensity in the line arising from the transmitted photospheric light. These numbers are proportional to the corresponding fluxes from these portions of the star, since these fluxes are obtained by multiplying R_1, R_2, and R_3 by the flux from the photosphere. Estimation of how the total residual intensity $R = R_1 + R_2 + R_3$ will change as different parts of the star are eclipsed then follows from Table 3.

My sincere thanks are due to Dr. S. Chandrasekhar for his criticism and guidance throughout this study, and to Dr. J. L. Greenstein for helpful discussions of the application of the theory to observation.